National Defense
Defence nationale

DRES

SUFFIELD MEMORANDUM

NO. 1223

AD-A202 206

REMOTE MINEFIELD DETECTION

USING

INFRARED LASER RADAR (U)

by

G.C. Stuart

PCN 031 SD

November 1988

DEFENCE RESEARCH ESTABLISHMENT SUFFIELD, RALSTON, ALBERTA

Canada

88 12 12 041

DEFENCE RESEARCH ESTABLISHMENT SUFFIELD

RALSTON, ALBERTA

SUFFIELD MEMORANDUM NO. 1223

REMOTE MINEFIELD DETECTION USING INFRARED LASER RADAR (U)

by

G.C. Stuart

DEFENCE RESEARCH ESTABLISHMENT SUFFIELD
RALSTON, ALBERTA

SUFFIELD MEMORANDUM NO. 1223

REMOTE MINEFIELD DETECTION USING INFRARED LASER RADAR (U)

by

G.C. Stuart

ABSTRACT

High-resolution infrared laser radars are shown to be effective sensors for use in remote minefield detection (RMD). The theoretical aspects and practical limitations of imaging laser radars are discussed and the conceptual designs of two airborne carbon-dioxide laser radars are presented. A design which uses direct detection and a linear-array detector is shown to be superior to one using heterodyne detection and a single-element detector. Countermeasures to active infrared RMD systems are discussed and suggestions made for further study.

TABLE OF CONTENTS

LIST OF TABLES   Page

LIST OF FIGURES   After Page

DEFENCE RESEARCH ESTABLISHMENT SUFFIELD

RALSTON, ALBERTA

SUFFIELD MEMORANDUM NO. 1223

REMOTE MINEFIELD DETECTION USING INFRARED LASER RADAR (U)

by

G.C. Stuart

1. INTRODUCTION

1.1 Motivation

Mine/countermine warfare plays an increasingly important role within modern land forces. Advances in mine fuzing and improvements in the destructive power of mines have made them more effective in both their anti-personnel and anti-vehicle roles. Of equal significance is the increased ability to rapidly deploy minefields using artillery, aircraft and ground vehicles. These scatterable minefields are significant obstacles on today's highly mobile battlefield. Paralleling the rapid development of mine warfare systems are new and more effective means of breaching minefields. As the capability to both lay and neutralize minefields improves, the need for new methods of minefield detection has arisen.

Scatterable mines are a serious threat to any moving armoured force. Consider, for example, the situation faced by the commander of an armoured column who needs to know whether or not a minefield lies ahead of his vehicles. Current information, gathered in real time, is required to avoid scatterable mines which the enemy may have recently deployed.

Remote minefield detection (RMD) provides a means of locating minefields from an airborne platform. The Ordnance Detection Group (ODG) at the Defence Research Establishment Suffield (DRES) is currently undertaking a research program which is investigating advanced RMD systems for use by the Canadian Military. Conventional aerial photography will continue to have important applications with respect to the detailed mapping of minefields but is not well-suited to the type of rapid combat operation under discussion here. A covert, all-weather, real-time sensor is required which can detect scatterable minefields at any time of the day or night. Airborne infrared (IR) laser radars have the potential to meet these RMD requirements.

The aim of this report is to review the important aspects of laser radars as they relate to the problem of remote minefield detection. A good understanding of the operating principles and characteristics of laser radars must be obtained before one can consider their use in any particular application. This report discusses the current state-of-the-art in carbon-dioxide laser radar and identifies key areas of technology and theory which must be investigated as part of the development of an RMD system.

1.2 Wavelength Considerations

The entire range of the electromagnetic spectrum may be exploited for the purposes of remote minefield detection. The need for a sensor capable of operating 24 hours a day can be met using active systems in the ultraviolet, visible, infrared and microwave spectral bands, and by using passive systems in the thermal infrared and microwave. The requirement for high-resolution effectively eliminates the potential of microwave systems for RMD. Visible wavelengths are inappropriate due to the need for covert operation and the relative ease of camoflaging mines in the visible. Active ultraviolet sensors suffer from problems of severe atmospheric attenuation and a lack of reliable, efficient laser sources. The thermal infrared, which describes the 8 μm to 14 μm wavelength band, appears to be the most promising for use in both active and passive RMD systems.

1.3 Infrared RMD Systems

An active thermal IR RMD system obtains an image of the scene below the aircraft by measuring reflected infrared radiation which has been generated by a source onboard the aircraft. Carbon-dioxide (CO_2) lasers serve as compact and efficient sources of coherent thermal IR radiation for an active RMD system. Th⁻ nominal CO_2 laser wavelength of 10.6 μm is within the excellent atmospheric window which gives thermal IR systems a degree of operational capability in a wide variety of environmental conditions. CO_2 lasers are used in a variety of military applications including rangefinders, target designators and imaging systems. CO_2 laser radiation is spectrally compatible with the technology of forward-looking infrared (FLIR) thermal imagers. These passive airborne sensors have gained widespread acceptance and have proved especially useful in the ground-attack and reconnaissance roles.

When applied to the problem of minefield detection active IR systems have certain advantages over their passive counterparts. Active thermal IR systems have much greater intrinsic signal-to-noise levels than passive systems which may allow them to function in adverse weather and penetrate the smoke, haze and dust of a battlefield. The contrast between mines and the background is more invariant for an active system, which is measuring reflectivities, than for a passive system which senses differences in thermal emittances. These emittances vary with both the time of day and the environmental conditions. The contrast in passive thermal IR measurements tends to follow the diurnal cycle, peaking twice a day and falling almost to zero at other times. Active systems are far more versatile in that they can readily be configured to give range and target-velocity information, making them useful for many other roles in addition to minefield detection.

Among the disadvantages of an active IR system are its increased complexity and somewhat greater vulnerability to enemy detection of the RMD aircraft. It may be easier to camouflage mines against active infrared sensors than passive systems. Table 1.1 presents a comparison of passive and active thermal infrared remote minefield detection.

1.4   Design Process

CO_2 laser radar systems have been developed and investigated for many diverse applications and sufficient information about the current technology of CO_2 laser radars exists to allow for a preliminary conceptual design of an active infrared RMD system. The design process itself indicates the critical aspects of the problem and serves to direct future experimental studies and verify theoretical concepts. It must be emphasized that the purpose of the conceptual design is to

TABLE 1.1

DIFFERENCES BETWEEN PASSIVE AND ACTIVE THERMAL IR RMD

	Passive IR	Active IR
basis of mine discrimination	thermal emmitance $f(\epsilon,T)$	reflectance
contrast	varies	constant
best contrast	hot mines/cold background	specular mines/ diffuse background
image quality	no speckle	speckle
multifunction	none	extensive
complexity	lesser	greater
vulnerability	lesser	greater
mine camouflage	difficult	retro-reflectance suppression

investigate the potential application of airborne infrared laser radar
to RMD rather than to attempt to develop the final system.

The designs of the RMD systems presented in this document focus
only on the acquisition of images suitable for processing and use in
the subsequent identification of the minefields. The actual image pro-
cessing equipment and algorithms will depend to a great extent on the
quality of the images obtained and the contrast between actual mines
and typical backgrounds.

1.5   Document Organization

This report deals with the development and application of high-
resolution CO_2 laser radars for use as the sensors of an active infra-
red RMD system. Section 2 presents a general discussion of the opera-
tional considerations, the airborne platform and the data processing
arrangement for the infrared laser radar RMD system. A more detailed
description of the geometry of the RMD scanning and of scatterable mine
targets is given in Section 3. Section 4 discusses the technology and
characteristics of CO_2 laser radars. The specifications of the pro-
posed RMD system and the details of two conceptual designs are pre-
sented in Section 5. Two fundamentally different approaches are taken
to the problem of obtaining active infrared images of sufficiently high
resolution to detect scatterable mines. The first design presented
mechanically scans the CO_2 laser beam and uses heterodyne detection
while the second system emits a fan beam and uses direct detection. In
both cases image data is collected line by line, with the forward
motion of the RMD aircraft providing the second dimension of the image.
Section 6 discusses the expected results when the airborne CO_2 laser
radars are used against a simple model of a scatterable minefield.
Countermeasures to active thermal RMD systems are discussed in

Section 7. The final section summarizes the results and recommends important areas for future in-depth analysis.

The use of infrared laser radars in RMD requires knowledge in a wide variety of subject areas including reflectance theory, speckle and infrared detection. Appendices A, C and E give this theory while other appendices provide further information relevant to CO_2 laser radars.

2.   RMD SYSTEM CONCEPT

2.1   System Operation

The three major components of a remote minefield detection system are the sensors, the airborne platform, and the image processing equipment. This report focuses on the sensors, namely high-resolution CO_2 laser radars, but it is useful to briefly consider the other elements of the RMD system and discuss its overall operation. The final design of a fieldable system must carefully balance the requirements of each of these separate factors, making compromises where necessary.

Figure 2.1 is a simplified block diagram of the RMD system operating in a typical situation. The active infrared sensors on board each of the remotely piloted vehicles (RPVs) scan the ground for scatterable mines. The image data and flight information, including RPV position, altitude and velocity are transmitted to the mobile ground control station (GCS). The images are processed in the GCS, which sends flight control signals to the RPV and distributes the minefield information. In this particular scenario the mobile ground station is supervising two RMD aircraft which are supporting a group of armoured fighting vehicles.
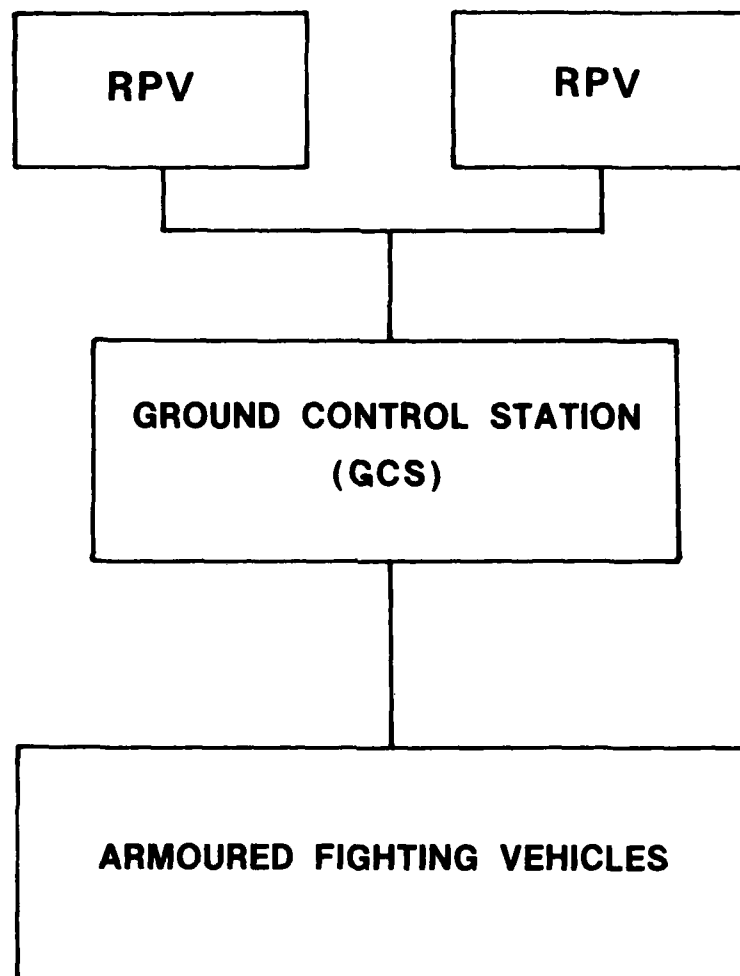
Figure 2.1

BLOCK DIAGRAM OF THE RMD SYSTEM

2.2   Airborne Platform

There are numerous advantages in using an RPV, rather than a manned-aircraft, as the platform for the remote minefield detection system. One of the principle benefits is the reduced risk of the surveillance personnel. An RMD platform flys relatively slowly, at a fixed low altitude, as it scans the terrain for mines. This makes it quite vulnerable to enemy anti-aircraft fire. Compared to a larger aircraft an RPV is significantly more difficult to detect and destroy because of its quietness and small cross-section at both visible and radar frequencies. Should the RPV be destroyed the loss, in terms of human life and monetary value, would be substantially less than would occur with a larger manned platform. Ideally the RPV-based RMD system will be inexpensive enough to allow deployment on a widespread basis within friendly forces. The total number of RMD aircraft must be fairly large so as to provide adequate coverage of the battlefield and absorb the inevitable losses which will occur during combat operations.

The same features of an RPV which make it an attractive platform for remote surveillance unfortunately also impose restrictions which will affect the final design of the RMD sensors. The limited payload of an RPV introduces severe constraints on the size and weight of the RMD apparatus. The CO_2 laser radar equipment, processing electronics and telemetry equipment must be very compact and light. These restrictions increase the already substantial difficulties of sensor stabilization which are common to all airborne laser radars.

2.3   Processing Considerations

One of the most fundamental decisions which must ultimately be made for any RMD system is to determine how much of the data analysis will be carried out on board the aircraft itself. The high-resolution imaging CO_2 laser radars gather vast amounts of data which must be processed and analyzed in near real-time. The necessary image processing equipment may be on the RPV itself, or located within the mobile ground station. Processing on the aircraft provides a greater degree of vehicle autonomy and reduces the problems associated with the sophisticated RPV/ground data link that would be required in order to transmit the raw image data. With onboard processing, transmissions between the ground and RPV are limited to control signals and "minefield/no minefield" results. The increased weight of the image processing hardware is offset by the reduced amount of communication equipment required on the RPV.

Processing on the ground requires a secure wideband data link between the RPV and its GCS. The RPV would be continuously transmitting infrared image data to the ground for analysis, increasing the susceptibility to enemy jamming and to RPV detection. Locating the image processing equipment on the ground allows for much more flexibility in that the weight and size of the processing computers becomes much less of a concern in the system design. Other advantages include the reduction of the electrical power requirements of the RPV, the potential for processing data from multiple sensors and the reduction in the cost of the comparatively vulnerable RPV. Table 2.1 summarizes the relative benefits of processing in the ground control station compared to processing in the RPV.

TABLE 2.1

SUMMARY OF FACTORS INFLUENCING PROCESSING LOCATION

	Processing on Aircraft	Processing in Ground Station
RPV vulnerability	lesser	greater
Data link	simple	complex
Multiple RPVs per GCS	no	yes
RPV flight control	no IR data	IR data

3.   REMOTE MINEFIELD DETECTION

3.1   Geometry

The actual geometry of the RMD problem is a critical factor in determining the overall performance of the imaging CO_2 laser radar. The operational altitude, angular resolution, total field-of-view (FOV), pixel size and swath width of the sensor are all interrelated. Note that throughout this report the terms pixel (picture element) and reselm (resolution element) will be used interchangeably.

Figure 3.1 shows the RMD aircraft flying at a height h over a flat area of ground. The total field-of-view of the sensor is 2ϕ, the

RPV

ϕ

θ

h

S

W

RESELM

ℓ

S
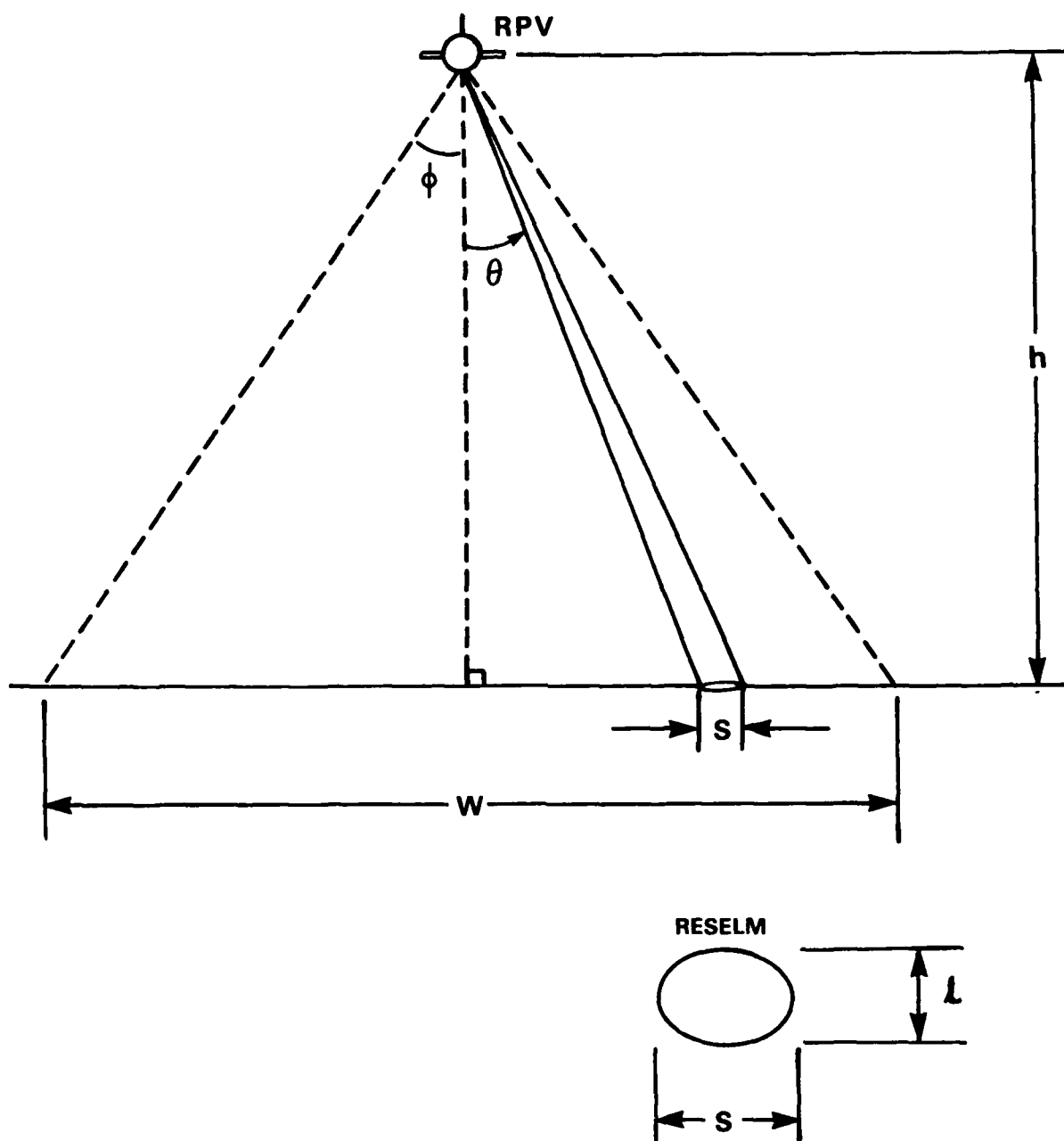
Figure 3.1

GEOMETRY OF RMD IMAGING

angular resolution of the system is δ, and the angle from nadir is θ.
The angular resolution and the total FOV have both been exaggerated in
this figure for the sake of clarity. The RPV is travelling out of the
page with a velocity of $\vec{v}_A$. At nadir the reselm on the ground is cir-
cular, with a diameter of hδ. At all other angle the pixels are ellip-
tical, with along-scan axes of $s = h\delta/\cos^2\theta$ and normal-to-scan axes of
$\ell = h\delta/\cos\theta$. The area of each reselm is thus

$$A_R = \pi(h\delta)^2/4\cos^3\theta.$$

An important consideration in any proposed RMD system is the amount of
ground which can be investigated in a given time. The total scan width
is $w = 2h\tan\phi$ and the RPV covers an area of wv_A per unit time. A nar-
row swath means that multiple adjacent passes must be made to cover the
required area, which greatly increases the likelihood that the RMD air-
craft will be detected and fired upon. Multiple passes also increase
the decision time of the commander who is trying to determine whether
or not to move his force through the particular area in question. The
swath must be sufficiently wide to provide a clear path for an armoured
column on a single pass.

3.2   Image Acquisition

The RMD systems discussed in this report use the motion of the
aircraft to provide the second dimension of the infrared image. Images
are thus acquired one line at a time. The two different approaches
used by the proposed RMD laser radars are briefly outlined here, with
more explicit descriptions given in the detailed designs of Section 5.
The two CO_2 laser radar designs have been characterized by their method
of infrared detection rather than by the different ways in which they
obtain images of the ground. ·

3.2.1   Heterodyne Detection System

The CO_2 laser beam and the instantaneous field-of-view (IFOV) of a single sensor element are scanned across the direction of aircraft motion by a rotating mirror system. The pixels in any particular scan-line are obtained sequentially, and for contiguous scanning the angular scan rate is $\dot{\theta} = 2v_A\phi/h\delta$ radians per second. The scanner axis is at an angle of $\zeta = h\delta/w$ radians to the flight path in order to compensate for the motion of the aircraft and give scan lines perpendicular to the aircraft direction. Figure 3.2 shows the geometry of the single-element scanning where the scanner is assumed to have an instantaneous flyback. The maximum percentage over-scan, which is of the order of $100[1/\cos\phi - 1]\%$, is shown as the cross-hatched area in the figure.

3.2.2   Direct Detection System

The output of the CO_2 laser is spread into a fan-shaped beam which sweeps along the ground under the aircraft as it moves forward. The return signal from the ground below the RPV is imaged onto a linear array of detector elements which is perpendicular to the direction of aircraft motion. All the pixels in one line of the image are therefore gathered at once. This technique is commonly known as the pushbroom method, and the arrangement is shown in Figure 3.3.

The radiometric sensitivity of a pushbroom system is greater than that of a scanned single-element detector since each element of the pushbroom detector integrates over a pixel for the entire line sample interval. In the mechanically-scanned system each pixel is only measured for a small fraction of this interval (approximately 10^{-3} for a 1024-pixel scanline). An important advantage of pushbroom scanners is that spatial measurements in the image are superior to those
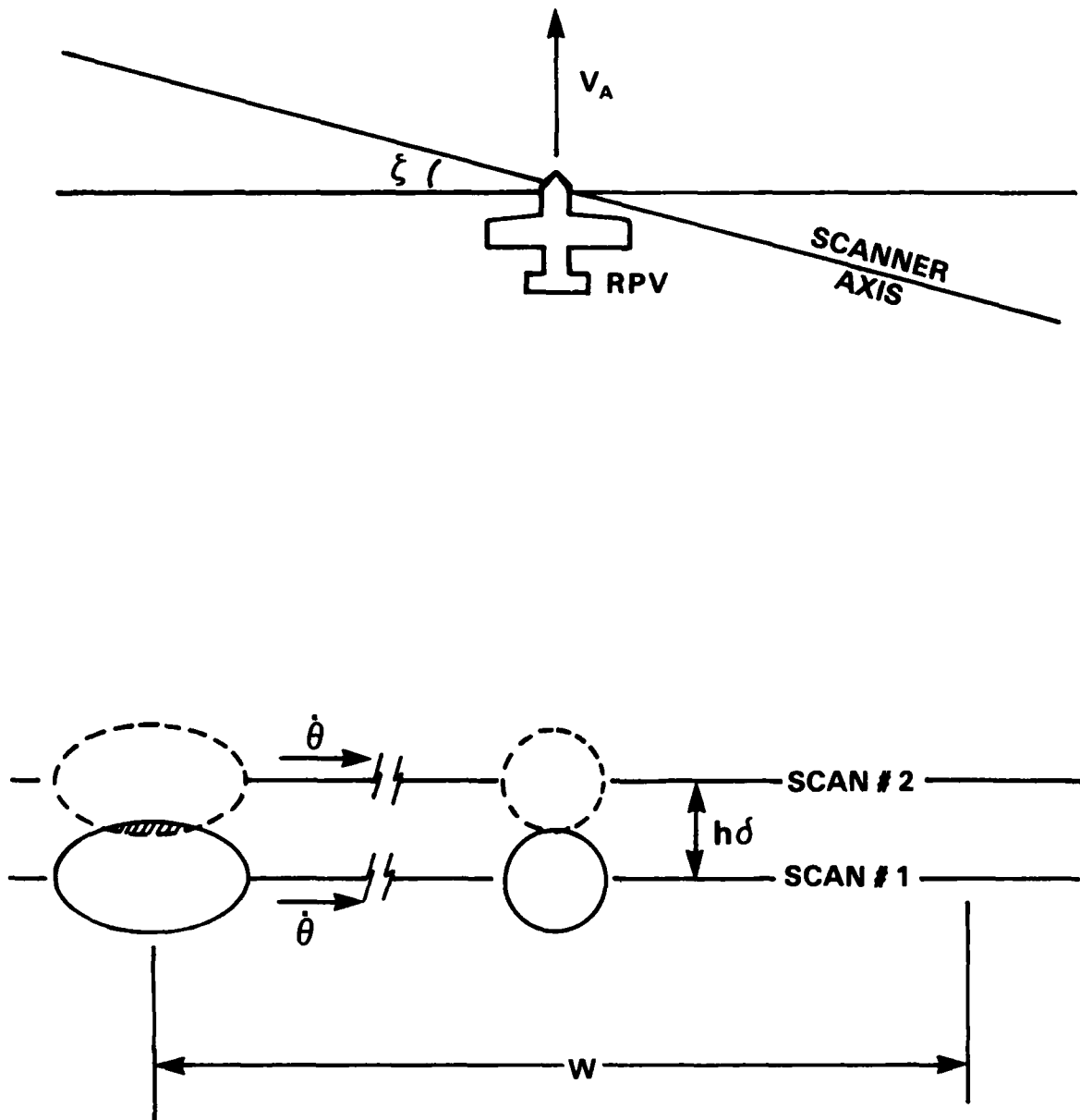
Figure 3.2

SINGLE-ELEMENT SCANNING

LINEAR ARRAY

RPV

V_A

ϕ

W
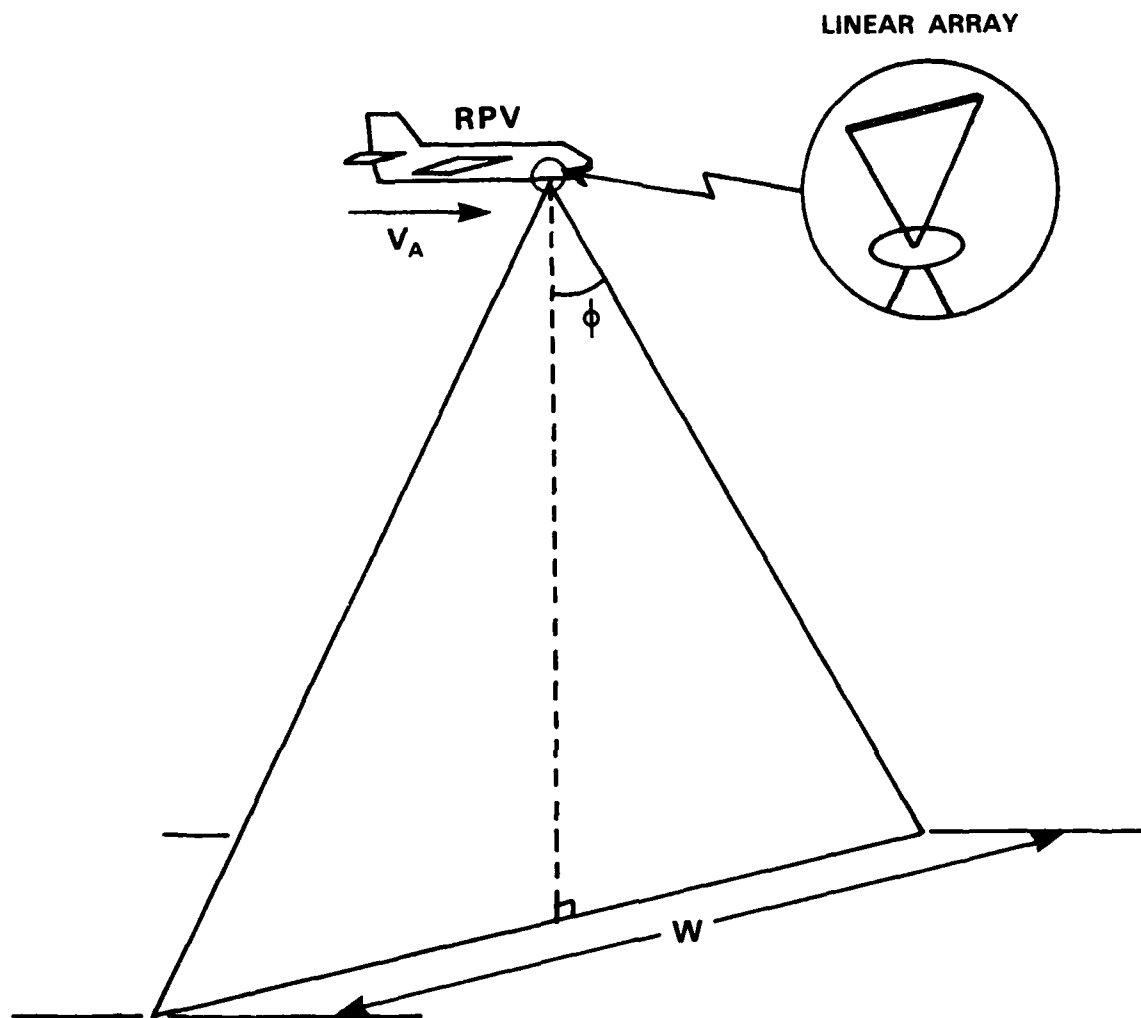
Figure 3.3

PUSHBROOM SCANNING

obtained with mechanical scanning, where imperfections in the rotating scan mirrors lead to geometric distortions in the image. Mechanically-scanned systems also introduce frequency broadening due to Doppler effects at the scanning mirror surfaces. The major disadvantage of a pushbroom arrangement is that it requires a sophisticated detector array and such arrays have only recently been developed for use at 8-13 μm infrared wavelengths.

3.3   Discrimination Methods

The successful application of CO_2 laser RMD requires that the mines be sufficiently distinct in relation to the surrounding background. Discrimination is based on assumption that the infrared reflectance of scatterable mines will be different from that of background materials. The reflectance of an object illuminated by coherent 10.6 μm radiation is a function of both the material and the surface roughness. Man-made objects are generally better specular reflectors in the thermal infrared than naturally-occurring targets such as grass, leaves and soil.

The major difficulty with downward-looking airborne laser radars is that of distinguishing between the two speckle distributions which occur when both the targets and the background are diffuse.

3.4   Scatterable Mine Targets

The intended targets of the RMD sensors are scatterable mines (SM) and the characteristics of these mines are clearly an important consideration. Scatterable mines tend to be somewhat smaller that conventional mine types, with diameters ranging from 5 cm for anti-personnel (AP) mines to 20 cm for anti-vehicle (AV) mines. For the

sake of this report the typical SM will be taken to be a squat, flat-topped cylinder of 15 cm diameter and 5 cm height.

Scatterable mines are either metal or plastic, and may be bare or painted. The model SM used in the RMD sensor designs is metal with a coat of olive drab paint. Figure 3.4 gives the angular dependence of the mine's retro-reflectance at 10.6 μm, and shows the predominantly specular nature of the reflectance distribution. This is not neces-sarily the case for all paints and the great variability in the reflectivity of standard camouflage paints is one of the most serious concerns about the future success of RMD. Mines have traditionally been camouflaged only at visible wavelengths, but, as discussed in a later section, detection by active IR may be countered by using specialized anti-IR-reflective coatings which are available.

The actual mechanism by which the scatterable mines are deployed provides additional information useful in RMD. Mines delivered from aircraft are frequently parachute-retarded. The para-chutes of these mines may also be detectable by a RMD system. Artillery-delivered mines are known to leave significant "skid marks" upon landing. In most cases, and with all types of SM, there is some degree of vegetation damage related to their deployment. High-resolution imaging RMD lidar systems can use this information as a further aid to minefield descrimination.
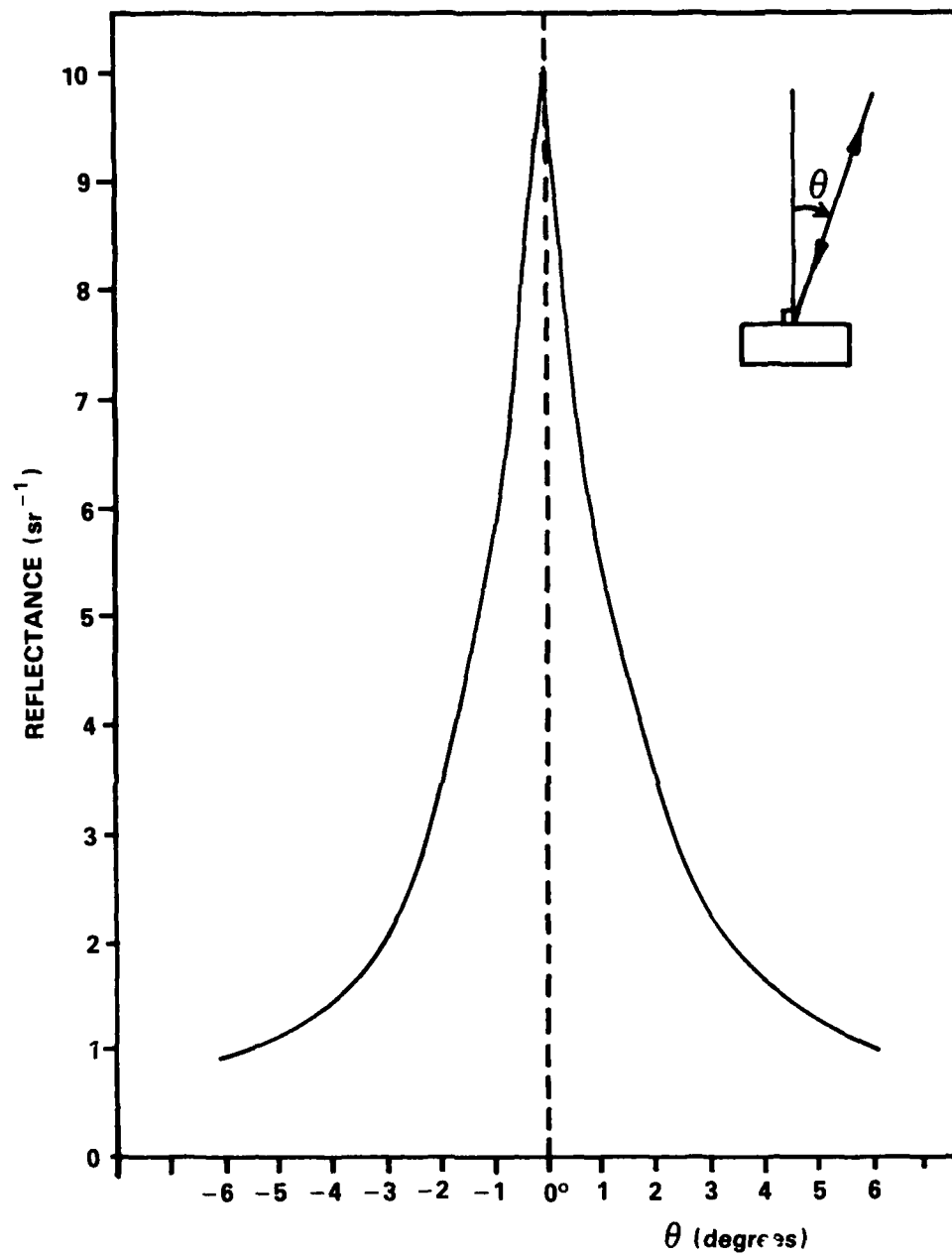
Figure 3.4

10.6 μm REFLECTANCE OF A MODEL SCATTERABLE MINE

4. LASER RADAR SYSTEMS

4.1 CO_2 Laser Radars

The problem of laser-based RMD is essentially one of applying high-resolution imaging radar methods to the specific task of detecting mines from a remote platform. High resolution is achieved by moving to optical frequencies which are defined here as being all frequencies greater than microwave but less than X-ray. This portion of the electromagnetic spectrum includes infrared, visible and ultraviolet light. The proposed RMD sensors operate in the thermal infrared and make use of the 8-13 μm atmospheric window.

Perhaps the first point to be discussed is the varied nomenclature of researchers working in optical RMD and in other closely-related fields. There are as many different ways of describing active systems as there are types of lasers and detectors. For example a CO_2 laser-based system can be called a ladar, a lidar, an optical radar, or an infrared radar. The most commonly used expressions are lidar and laser radar.

Much of the terminology of laser radar has been taken from conventional mm-wave radar, and discussions frequently involve terms such as radar cross sections and antennas. The fundamental lidar equation is the familiar radar equation,

$$P_S = P_T \rho A_o \kappa / \pi r^2 \exp[-2(\alpha+\gamma)r]$$

where P_T and P_S are the transmitted and received laser powers, ρ is the target reflectivity, A_o is the area of the receiving optics, κ is the optical efficiency of the system, r is the target range, α is the

atmospheric absorption coefficient, and γ is the atmospheric scattering coefficient. This equation is valid for an extended diffuse target which is larger than the instantaneous field-of-view of the laser radar. The optical efficiency factor accounts for the losses in the two-way transmission of radiation through the optical system. At 10.6 μm typical values of the atmospheric coefficients for very clear conditions are $\alpha = 0.125$/km and $\gamma = 10^{-4}$/km. Table 4.1 presents attenuation coefficients[1] for the 10P(20) laser line in a variety of weather conditions and Figure 4.1 shows the probability distribution of 10.6 μm attenuation[2] measured in Europe. Standard atmospheric models have been developed which allow for calculation of these wavelength-dependent coefficients (for example the well-known LOWTRAN computer code developed by the US Air Force Geophysics Laboratory).

A CO_2 laser radar, operated in a monostatic configuration, is shown in Figure 4.2. The transmitted laser beam and the received radiation share a common telescope and object-space scanner. Polarization discrimination techniques are used to differentiate between the outgoing and incoming signals. A quarter-wave plate converts the transmitted CO_2 laser beam from linear to circular polarization. The received radiation from the target is again made linearly polarized when it passes through the quarter-wave plate but now the direction of the polarization is perpendicular to that of the original laser output. Brewster-angled optics are then used to direct the received signal to the detector.

Monostatic laser radars are prone to problems of backscatter from the telescope optics but this can be controlled though the use of eccentric pupil telescopes such as that in Figure 4.3. Unfortunately it is difficult to design eccentric pupil telescopes with fields-of-view greater than three degrees. Time-of-flight considerations can be

TABLE 4.1

ATMOSPHERIC ATTENUATION COEFFICIENTS FOR A WAVELENGTH OF 10.6 μm

	absorption coefficient α (km^{-1})	scattering coefficient γ (km^{-1})
MOLECULAR COMPONENT		
tropical	0.58	<10^{-6}
midlatitude—summer	0.36	<10^{-6}
—winter	0.08	<10^{-6}
subartic—summer	0.20	<10^{-6}
—winter	0.04	<10^{-6}
AEROSOL COMPONENT		
clear	0.0055	0.008
hazy	0.0270	0.039

[adapted from: Handbook of Optics[1]]
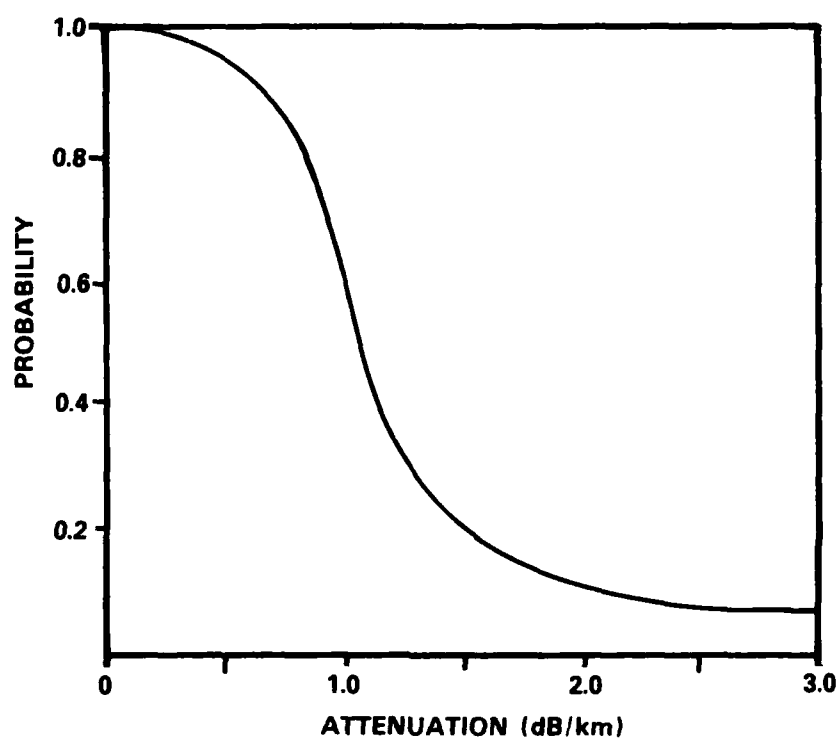
Figure 4.1

ATTENUATION PROBABILITY AT 10.6 μm IN EUROPE
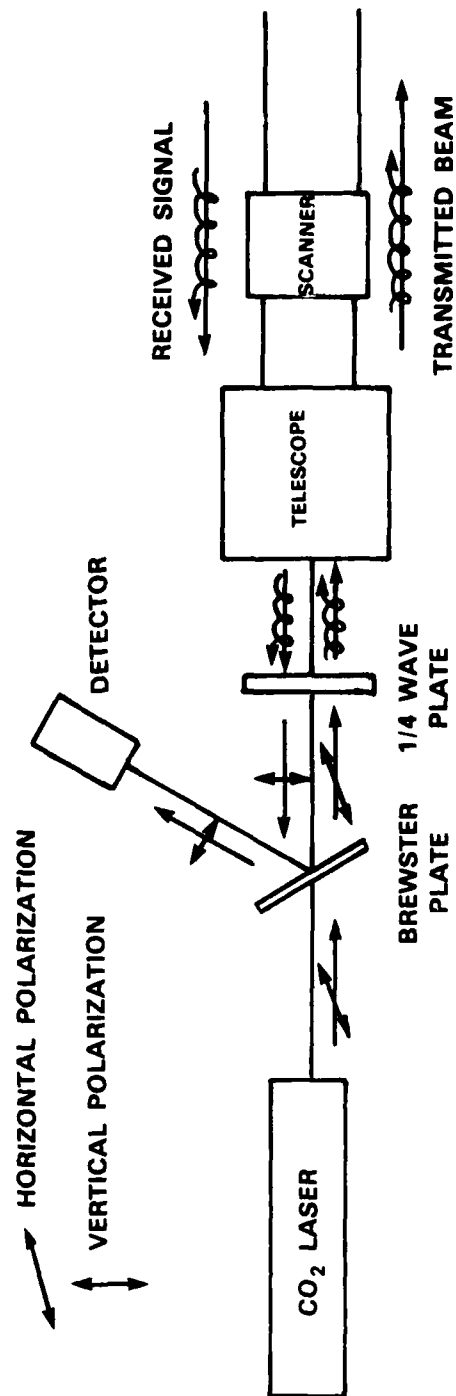
Figure 4.2

MONOSTATIC CO$_2$ LASER RADAR
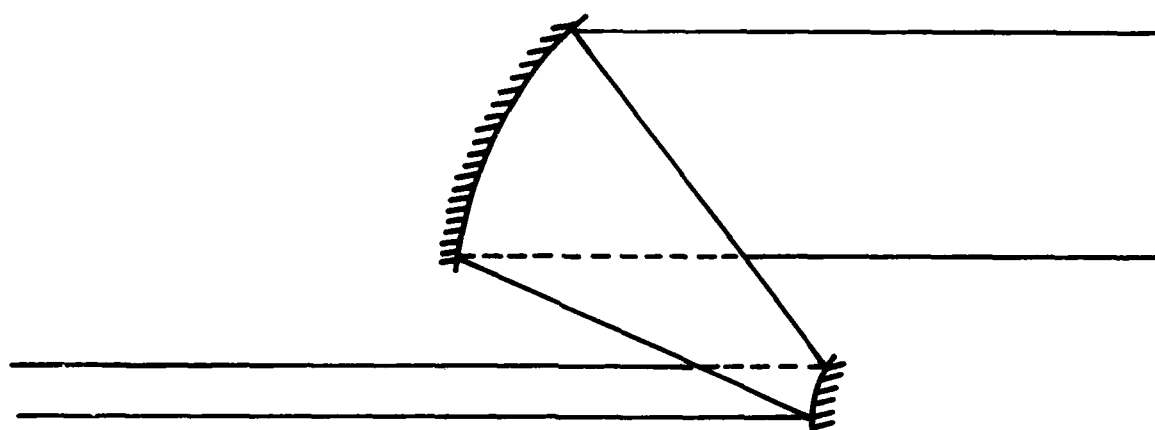
Figure 4.3

ECCENTRIC PUPIL TELESCOPE

very important in laser radars, especially those using high-speed scan-
ners. The transmitted CO_2 laser beam must lead the receiver field-of-
view in order to achieve correct registration.

Many CO_2 laser radars have been constructed and their charac-
teristics studied and compared with theoretical limits. One of the
most common applications are differential absorption lidar (DIAL)
systems which use dual wavelengths to measure trace constituents in the
atmosphere. In fact many of the studies of IR reflectance have been
motivated by the need to obtain accurate data on DIAL target materials.
CO_2 DIAL has demonstrated its potential as an effective sensor for the
remote detection of chemical warfare agents. In addition to DIAL
systems, CO_2 laser radars have been used in rangefinding, geologic map-
ping, and in a number of imaging applications. Table 4.2 presents the
characteristics of a number of ground-based CO_2 laser radars while
Table 4.3 gives a selection of airborne laser radar systems. The
acronyms used in the tables are described in Appendix J, but it is use-
ful to note here that PC and PV are photoconductive and photovoltaic,
and PRF is the pulse repetition frequency.

Most of the monochromatic laser radars operate on the 10P(20)
line, which corresponds to a wavelength of 10.591 μm, while the DIAL
systems use tuned pairs of wavelengths in the 9 μm and 10 μm bands. A
wide variety of CO_2 laser transmitters are used, including low-pressure
continuous-wave lasers and high-pressure pulsed lasers. Airborne
systems are frequently built around compact waveguide CO_2 lasers. In
addition to the laser and detector information Table 4.3 gives the
velocity-to-height ratios for the airborne laser radars.

Detection of the return infrared signals is performed by either
direct or heterodyne techniques, and mercury-cadmium-telluride (HgCdTe)

TABLE 4.2

GROUND-BASED CO$_2$ LASER RADARS

Ref.	CO$_2$ laser	Detection	Resolution δ (mrad)	Aperture (cm)	Range (km)	Description
3	0.1 Hz PRF 1 J pulses	het. and dir. HgCdTe	0.3	20	2	aerosol backscatter
4, 5	TEA, 1 Hz PRF 200 mJ pulses	dir. PV HgCdTe	0.8	14	0.2 0.077	imaging, 32 x 24 pixels non-imaging
6	hybrid TEA, 1 Hz PRF	het. PV HgCdTe	0.13	10	5	rangefinder
7	TE, 1 Hz PRF	dir. PC HgCdTe	0.45	7	10	rangefinder
8	50 W cw	het. PC Cu:Ge 4.5 MHz	0.2	5.8	8	line-scanner
9	4 W cw, rf waveguide	het. HgCdTe 120 MHz	3	1	1.4	imaging, Doppler MTI 25 x 25 pixels
10-12	2.5 W cw, freq. modulated	het. PV HgCdTe 100 MHz	0.2	10	10	imaging
13	5 W cw	het. HgCdTe				spot focus at target
14	TEA, 500 Hz PRF	HgCdTe	1.1	30	2.7	DIAL
15	TEA, 100 Hz PRF	dir. PC HgCdTe, het. PV HgCdTe	0.5	10	2.7	DIAL
16-19	Q-switched 25 kHz PRF	het. PV HgCdTe	0.1	10	2.7	imaging, 128 x 128 pixels, IRAR testbed
20	4 W cw	het. PC	0.3	5	7	rangefinder
21,22	hybrid TEA 20 Hz PRF	het. HgCdTe		28	>1.5	Doppler weather
23	5 W cw waveguide	heterodyne	0.4	5	0.5	imaging

TABLE 4.3

AIRBORNE CO_2 LASER RADARS

Ref.	CO_2 laser	Detection	Resolution δ (mrad)	Aperture (cm)	v/h (ms^{-1}/ km)	Description
24	2.5 Hz PRF 100 mJ pulses	direct	1	9	100 / 2	DIAL
25	cw	heterodyne	1	-	- / 3	DIAL
26, 27	3 W cw	het. PbSnTe	0.3	7.5	50 / 0.5	geologic mapping, dual wavelength
28	40 kHz PRF	het. PV HgCdTe 3 MHz	0.25	10	- / 1.6	helicopter wire-avoidance
29	4 W cw freq. modulated	het. HgCdTe	1	5	16 / 0.15	helicopter 4000 pixel image
30	30 kHz PRF	het. PV HgCdTe	0.5	17	-	helicopter 350 x 175 image
31	3 W cw waveguide	het. PV HgCdTe 100 MHz	0.1	15	-	airspeed, LATAS velocimeter
32	pulsed	dir. PC HgCdTe	4	10	60 / 0.5	geologic mapping multi-wavelength
33	40 W cw rf waveguide	het. PV HgCdTe 100 MHz	0.1	13	250 / 0.06	imaging, MICOS ground attack

is by far the most prevalent detector material. HgCdTe detectors are cooled to liquid nitrogen temperatures in most cases. All the detection bandwidths given in Tables 4.2 and 4.3 represent those of the detector + amplifier combination. Photovoltaic HgCdTe detectors can have intrinsic bandwidths in excess of a GHz. Range-gated detection is often used in imaging CO_2 laser radars to reduce background effects. Unfortunately range-gated imaging is of limited use when downward-looking airborne laser radars are targeting small objects lying on rough, irregular ground and range-gating is not applicable to remote minefield detection.

The angular resolutions quoted in the tables are the instantaneous fields-of-view of the detectors. In the case of diffraction-limited systems, if λ is the wavelength, and D is the diameter of the lidar optics, the angular resolution is given by $1.22\lambda/D$. The use of detector arrays in laser radars can increase the angular, spatial and spectral coverage while maintaining or reducing the specifications for the scanners, lasers and individual detector bandwidths. Heterodyne lidars using arrays must resort to sophisticated techniques such as holographic beam-shaping[36] to ensure that the local oscillator correctly illuminates each element of the array. The transmitted spot on the target must also be matched to the detector footprint. When d is the diameter of each element of the array, b is the center-to-center spacing of the elements, and f is the focal distance, the number of detectors in the focal-plane array must be less than $\lambda f/db$. This condition satisfies the antenna theorem for coherent detection. High-magnification lidars cannot use image-plane scanning because of the limited overall field-of-view. In the case of heterodyne systems the image-plane scanning FOV must be equal to the diffraction-limited FOV.

CO_2 laser radar technology has found a number of military applications including rangefinders, systems for detecting chemical warfare agents, and imagers for target detection, identification and tracking. Airborne infrared laser radars have been developed for terrain following and wire-avoidance. This latter application is particularly important for helicopters and other low-flying aircraft operating in Europe. Coherent laser radar systems, which readily give the range and velocity of targets, are very useful sensors on tactical ground-attack aircraft, especially in the anti-armour role. Much of the interest in high-resolution airborne CO_2 lidars is directed to their use during close-air support missions. The IRAR (Infrared Airborne Radar) and MICOS (Multifunction Infrared Coherent Optical Sensor) programs[16-19,33-35] developed an imaging CO_2 laser radar for the A-10 Thunderbolt anti-tank aircraft.

4.2   Detection Methods

There are two fundamentally different types of detection used in optical radar systems. The first is coherent (heterodyne) detection, and the second is incoherent (direct) detection. The choice of detection technique is one of the most important factors determining a lidar's versatility, size and complexity. The first RMD sensor design, presented in Section 5.2, uses heterodyne detection and a continuous-wave (CW) CO_2 laser while the second design, described in Section 5.3, uses direct detection and a pulsed CO_2 laser. These represent only two of the many possible combinations of laser type, detection method and image collection scheme. Table 4.4 presents the practical options for an imaging RMD laser radar, where χ and Υ indicate heterodyne and direct detection. The only situation where CW lasers cannot be used is with the case of direct detection combined with a non-scanned multi-element detector array. There is insufficient CO_2 laser power density

on the target in this particular arrangement. Pulsed lasers are only
needed with fixed multi-element detectors and are not required in
scanned systems unless range information is required and direct detec-
tion is being used.

The fundamental differences between heterodyne and direct
detection laser radars are summarized in Table 4.5. D is the diameter
of the collecting optics, d is the diameter of the detector, λ is the
wavelength, and f is the focal length of the collecting lens. Two of
the most critical differences between heterodyne and direct detection
are in the areas of noise and the effects of speckle.

4.2.1   Noise

The power signal-to-noise ratio (SNR) for a CO_2 laser radar,
neglecting speckle and turbulence noise, can be expressed as

$$SNR = \frac{P_S}{A_d B/D^{*2} P_S + E_\lambda B/\eta}$$

where the first term in the denominator represents detector noise and
the second term is the signal photon-induced shot noise. These noise
sources are considered in Appendix E and in the following two subsec-
tions. P_S is the signal power, A_d is the detector area, B is the band-
width of the detection system, and D^* is the normalized detectivity.
Note that throughout this report signal-to-noise ratios will refer to
the power SNR unless otherwise indicated.

TABLE 4.4

OPTIONS FOR DETECTION IN IMAGING RMD LASER RADAR

	Pulsed Laser	CW Laser
scanned single-element detector	-	χ^1, Υ
scanned multi-element detector	-	χ, Υ
fixed multi-element detector	χ, Υ^2	χ

Note: ^{1} and ^{2} are the two RMD system designs discussed in this report

TABLE 4.5

COMPARISON OF HETERODYNE AND DIRECT-DETECTION LASER RADARS

	heterodyne	direct
angular resolution	$\approx \lambda/D$	d/f
noise	signal photon noise limited	Johnson and thermal background noise limited
small-signal SNR	$\eta P_S/E_\lambda B$	$P_S^2 D^{*2}/A_d B$
speckle	no averaging	aperture averaging
multifunction	extensive	limited

When the signals are large the signal photon noise is dominant and the SNR is proportional to P_S. For the situation where a CO_2 laser radar is targeting a diffuse surface the signal power P_S is inversely proportional to the square of the target range r. Both heterodyne and direct detection laser radar systems have large-signal SNRs which therefore go as $(1/r^2)$. However for small signals the detector noise dominates a laser radar which uses direct detection while the signal photon shot noise remains the limiting noise in a heterodyne detection system. The advantage in heterodyne detection is that its small-signal SNR is proportional to $(1/r^2)$ whereas that of direct detection is proportional to P_S^2 and hence to $(1/r^4)$. The maximum range of a heterodyne sensor is greater than its direct-detection counterpart.

CO_2 lidar experiments have demonstrated the much greater inherent sensitivity of heterodyne detection. The sensitivity can be described by using the noise-equivalent power (NEP), and Killinger[15] measured a direct NEP of 4nW while the heterodyne NEP was 2pW. The advantage in sensitivity of heterodyne detection is countered by its poorer performance in terms of speckle noise.

4.2.2   Speckle

Speckle noise is one of the most serious problems with CO_2 laser radars. Speckle, which is fully discussed in Appendix D, is random, high contrast noise due to the interference effects which occur upon the scattering of the infrared light from rough surfaces. The probability distribution functions for speckle statistics are dependent on the nature of the target. Totally diffuse targets have Rayleigh statistics for the scattered field amplitude;

$$P(E) = E/\sigma^2 \exp[-E/2\sigma^2]$$

where E is the amplitude of the electric field and σ is the standard deviation. Diffuse targets with glints have Rician distributions;

$$P(x) = xI_0(\hat{a}x)\exp[-(x^2+\hat{a}^2)/2]$$

where $x = E/\sigma^2$, $\hat{a}$ is amplitude of the glint in the received signal, and I_0 is a zero-order modified Bessel function.

Heterodyne detection systems must, by definition, have speckle signal-to-noise ratios of unity. Direct detection, which responds to the intensity of the fields rather that their amplitudes, can use aperture averaging to reduce speckle noise.

4.3   Heterodyne Detection

Optical heterodyne (coherent) detection[37-39] is possible due to the long coherence length and high frequency stability of CO_2 laser sources. Heterodyne detection requires stringent phase-front alignment and CO_2 laser radars using this technique are always diffraction-limited. In keeping with usual convention, heterodyne refers to the coherent mixing of two laser beams, regardless of their source. It should be noted that some authors reserve the term heterodyne for situations where there are two separate laser sources and use homodyne to describe systems which use a single laser and a frequency shifter to produce the local oscillator (LO) beam.

Consider the situation of Figure 4.4, which illustrates a typical geometry for an optical heterodyne receiver. The signal and the radiation from the local oscillator laser are combined at the photo-detector using a beamsplitter. The detector has a diameter of d and an area A_d. Optical heterodyning is constrained by the antenna theorem[40],
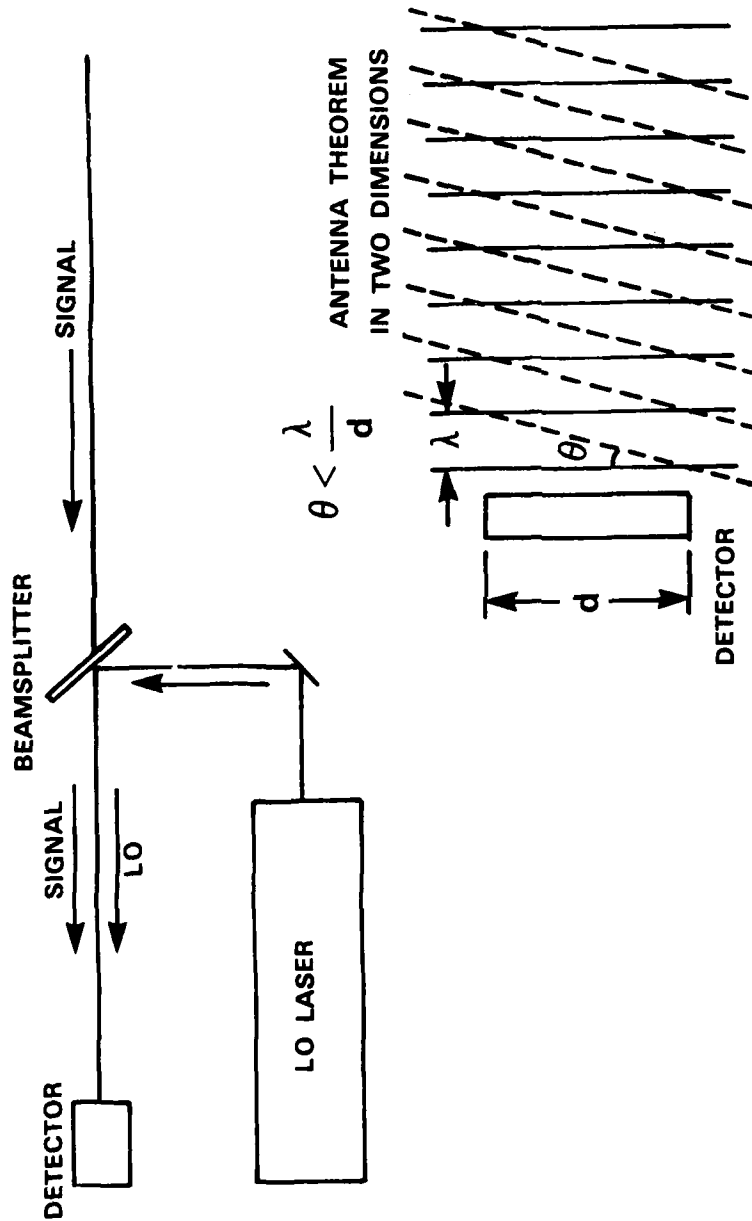
Figure 4.4

HETERODYNE RECEIVER GEOMETRY

which describes the required alignment between the wavefronts of the
signal and local oscillator beams. If Ω is the solid angle field-of-
view of the detector then the antenna theorem requires that $A_d\Omega \approx \lambda^2$.
The limited field-of-view corresponding to a given detector area
ensures that the signal and oscillator wavefronts will not be more than
a wavelength apart across the entire surface of the detector. The
effective aperture is large for small fields-of-view and, conversely,
is small given a large field-of-view.

The signal in the heterodyne detector results from the coherent
mixing of the electric field of the radiation from the target, $\vec{E}_S(\vec{r},t)$,
with that due to the local oscillator, $\vec{E}_{LO}(\vec{r},t)$. If ν_s is the fre-
quency of the incident target signal, and ν_{LO} is the frequency of the
local oscillator, then the term of interest in the output of the detec-
tor is at the difference frequency $(\nu_s-\nu_{LO})$. This signal is referred
to as the intermediate-frequency (IF) signal.

If θ_p is the angle between the local oscillator and signal
polarizations, the mean-square IF signal is,

$$\langle i^2 \rangle = 2\beta(\eta e/E_\lambda)^2 \ P_{LO}P_S\cos^2\theta_p$$

where P_{LO} and P_S are the oscillator and signal powers. The term
$(\eta e/E_\lambda)$ is the current responsivity of the detector (see Appendix E).
η is the detector's quantum efficiency, e is the fundamental charge,
and E_λ is the photon energy. For optimum heterodyne detection the
phase and amplitude of the local oscillator beam and the signal must be
correctly matched at the detector. Good matching results in an
improved signal-to-noise ratio, better angular resolution and less
focal-plane heating. β is a mixing efficiency factor which is a mea-
sure of how well the local oscillator and the signal are matched. For

a Gaussian signal profile and a plane-wave (uniform) LO beam the maximum possible value of β is 0.74. This occurs when the detector size is 70% of the size of the signal spot. The mixing efficiency can reach 84% when the LO beam is Gaussian and the signal and LO spots overlap. Figure 4.5 gives the mixing efficiency as a function of the overlap with the local oscillator beam.

Heterodyne detection laser radars are inherently polarization-sensitive and high local oscillator powers are desirable. When the power of the signal from the target is much less than the LO power the detection noise is dominated by the photon-induced shot noise due to the local oscillator radiation. This LO photon shot noise is,

$$\langle i^2 \rangle_{SN} = 2\beta e^2 (\eta/E_\lambda) P_{LO} B$$

where B is the frequency bandwidth of the detector system. The optical power of the local oscillator at which the thermal noise become equal to the shot noise is

$$P_{LO} = 2/\eta (k_B T/e)(E_\lambda/e) 1/R$$

where k_B is Boltzmann's constant, T is the temperature, and R is the electrical resistance of the system. For local oscillator powers greater than this value, typically a few milliwatts, the photon shot noise dominates and can be used to determine an estimate of the signal-to-noise ratio. The local oscillator power is ultimately limited by the damage threshold of the photodetector material. In the case of photovoltaic mercury-cadmium-telluride (HgCdTe) the damage threshold is of the order of $5W/cm^2$.
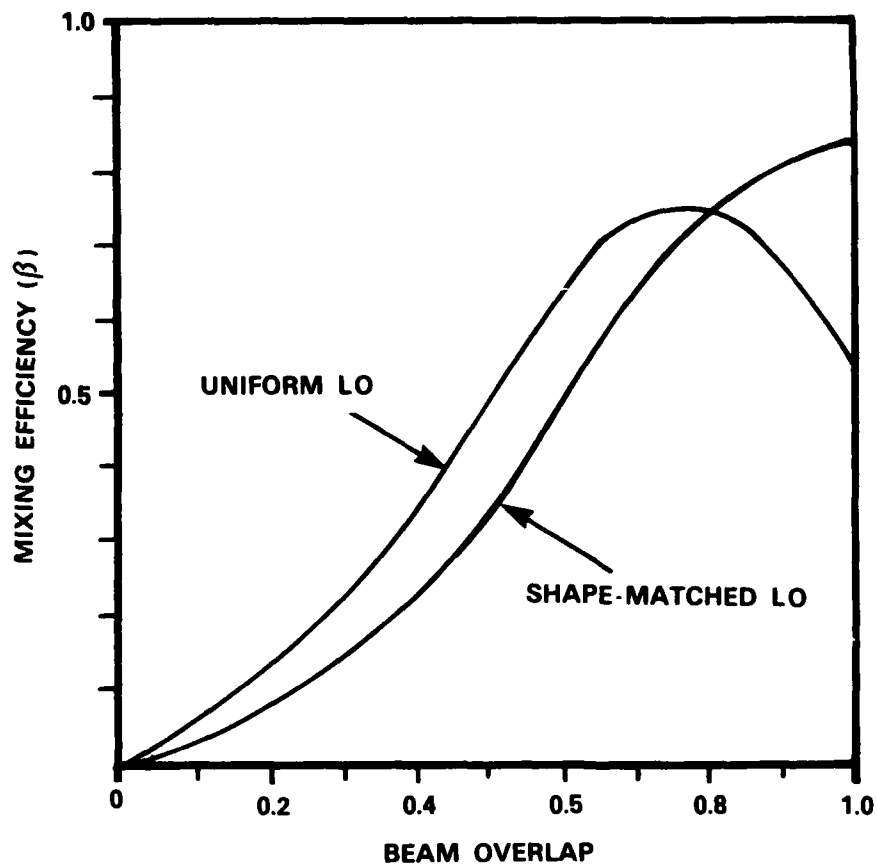
Figure 4.5

MIXING EFFICIENCY OF HETERODYNE DETECTION

The signal-to-noise ratio for the heterodyne detection system is

$$SNR = \langle i^2 \rangle / \langle i^2 \rangle_{SN} = \eta P_S \cos^2\theta_P / E_\lambda B.$$

Heterodyne detectors are insensitive to incoherent thermal radiation. The signal-to-noise ratio for the detection of a thermal source is

$$SNR = \eta / [\exp(E_\lambda / k_B T) - 1].$$

For a SNR of one, the temperature of the target must be

$$T = E / k_B [\ln(1+\eta)].$$

In the case of infrared radiation with a wavelength of 10.6 μm, and assuming unitary quantum efficiency, this temperature is 1960 Kelvin (1687°C). Heterodyne detection can not be used to obtain passive imagery in remote minefield detection since the temperature of the targets and background will be of the order of 300 K or less.

4.4   Direct Detection

Unlike microwave and radio frequencies the energy of a photon at infrared wavelengths is sufficiently large to make direct detection feasible. A 10.6 μm photon has an energy $E_\lambda = 0.12$ eV which is much greater that the $k_B T = 0.007$ eV energy of the phonons in a 77 K photodetector. Direct detection is relatively straight-forward compared to heterodyne detection, with the major differences being its more flexible field-of-view, greater noise, and the aperture averaging of speckle effects.

For small signals the direct-detection signal-to-noise ratio
is

$$SNR = \frac{P_S^2}{A_d \, B/D^{*2}}$$

where the detection is limited by the Johnson (thermal) noise in the
detector material itself and by the photon-induced shot noise due to
background infrared photons. Both these sources of noise are included
in the D* detectivity, and are further discussed in Appendix E.

5.   RMD SYSTEM DESIGN

5.1   Common System Specifications

Comparison of the two RMD sensor designs is only meaningful in
light of the many common parameters shared by both approaches to the
problem. The angular resolution of both the RMD laser radars is
$\delta = 0.256$ mrad. In the case of the scanned heterodyne system δ also
represents the instantaneous field-of-view (IFOV) and is the diffrac-
tion limit of the CO_2 laser radar. The total field-of-view of both of
the infrared laser radars is 15 degrees, the RPV velocity is
$v_A = 180$ kph, and the flight altitude is h = 100 m. The swath width is
26.3 m and there are 1024 pixels per scan line. The nominal pixel size
of 2.6 cm means that there of the order of five reselms across the
diameter of the model scatterable mine.

The CO_2 lasers of the lidar transmitters operate on the 10P(20)
rotational line, which corresponds to a wavelength of $\lambda = 10.591$ μm and
a frequency of $\nu = 28.3$ THz. The energy of each infrared photon is

0.12 eV. The 10P(20) line is chosen for several reasons, the primary considerations being the wide availability of reflectivity measurements at this wavelength and the superior gain of CO_2 lasers running on this particular line. An eight-bit digital value is assigned to each pixel and the data-gathering rate of each of the CO_2 laser radars is 1.97 million pixels per second.

The power of an incoherent-detection laser radar transmitter must be sufficient to overcome the background thermal radiation from the ground as well as the background flux from the optics, detector housing, and other components of the lidar itself. Assuming that the ground is blackbody source with a temperature of 300 K, Planck's equation gives a total emitted radiance of 0.146 W/cm²sr. The radiance within a 2 μm wide spectral window centered at 10.6 μm is 0.0016 W/cm²sr. If the laser radar receiver is taken to have an ideal bandpass corresponding to this spectral band an estimate of the thermal background noise can be made. In the case of the direct detection system the 2 μm bandpass is achieved by using a cooled spectral filter. If the emittance of the ground, ϵ, is not unity then the background radiance is given by,

$$L_B = 0.0016\ \epsilon\ \text{W/cm}^2\text{sr}$$
$$= 0.0016\ (1-\rho)\text{W/cm}^2\text{sr}$$

where ρ is the hemispherical reflectance (albedo).

If δ is the total cone angle representing the receiver field-of-view, the corresponding solid angle is $\Omega = \pi \sin^2(\delta/2)$ and the irradiance due to an Lambertian source of radiance L_B is

$$E_B = \pi L_B \sin^2(\delta/2).$$

The power due to thermal background emissions from the ground for a
receiver aperture area of A_o is therefore

$$P_B = A_o \Xi_3$$
$$= 0.0016\pi(1-\rho)A_o\sin^2(\delta/2).$$

When the reflectance of the ground is 10%, the receiver aperture has a
diameter of 5 cm, and the field-of-view is 0.256 mrad, this expression
gives a thermal background power of 0.58 nW.

The value of 0.58 nW is used to estimate the thermal background
noise power for both the heterodyne and the direct detection CO_2 laser
radar designs. The direct detection system, with its linear focal-
plane array detector is assumed to be ultimately limited by this back-
ground noise since the Johnson noise in a 1 GHz photodetector cooled to
77 K is only of the order of 4 pW. The heterodyne detection system,
with its single element detector is assumed to be limited by the
photon-induced shot noise due to the local oscillator radiation. This
LO photon noise power is 2.6 nW for a 2 MHz, 1 MΩ photovoltaic detector
with a 70% quantum efficiency, a 70% mixing efficiency, and for 1 mW of
local oscillator power.

Table 5.1 summarizes the common specifications for the two RMD
sensor designs. Both CO_2 laser radars have 5 cm diameter receiving
optics which corresponds to a solid angle of 1.963 (10^{-7}) radians. The
details of the heterodyne and the direct detection designs are
presented in the following two subsections.

TABLE 5.1

COMMON RMD SENSOR SPECIFICATIONS

Total Field-of-View, $2\emptyset$	= 15° [261.8 mrad]
Angular Resolution, δ	= 0.256 mrad [0.01465°]
Number of Pixels/Scan Line	= 1024 [2^{10}]
Aircraft Height, h	= 100 m
Aircraft Velocity, v_A	= 180 kph [50 m/s]
Swath Width, w	= 26.3 m
Nominal Pixel Size, s	= 2.6 cm
Laser Wavelength, λ	= 10.591 μm [10P(20) line]
Laser Frequency, ν	= 28.3 THz
Laser Photon Energy, E_λ	= 0.12 eV [$1.88(10^{-20})$J]
Total Time-of-Flight, tof	= 0.667 μsec
Pixel Dwell Time, τ	= 0.51 μsec
Receiver Aperture, D	= 5 cm
Receiver Area, A_o	= 19.63 cm²
Collection Solid Angle, Ω	= $1.963(10^{-7})$rad
IFOV Background Power, P_B	= 0.58 nW
Data Gathering Rate,	= 1.97 Mpixels/s [15.75 Mbits/s]

5.2   Coherent Sensor Design

The RMD heterodyne detection sensor uses rotating polygonal
mirrors (see Figure 5.1) to scan the instantaneous field-of-view of a
photodetector and the output from a continuous-wave CO_2 laser. Each
polygonal mirror has 48 facets and a radius of 6.1 cm. The transmitted
laser beam uses acousto-optic facet-following to maintain the beam on
the center of each 8 mm wide facet. Appendix F gives further informa-
tion on polygons and acousto-optic scanners. The transmit and receive
polygons are slightly offset so as to account for the 0.667 μsec time-
of-flight which occurs when the RPV is flying at an altitude of 100 m.
The detector is a single, circular, photovoltaic (PV) HgCdTe element,
cooled to 77 K, which has a radius of 0.1 mm. The quantum efficiency
of this 1 GHz PV HgCdTe detector is η = 70%, and its resistance is
1 MΩ. The optical efficiency of the laser radar is taken to be
κ =20%.

The CO_2 laser is an rf-pumped waveguide laser with a closed-
cycle gas system which emits 15 W of linearly-polarized 10.591 μm
radiation. A fraction of the output of this laser is split from the
main beam and passed through an acousto-optic frequency shifter to pro-
vide 1 mW of local oscillator power. The frequency difference between
the transmitted and LO beams is 10 MHz. The power at the exit of the
5 cm-aperture telescope is 10 W, and the beam divergence is 0.3 mrad.
A focal length of 55 cm ensures optimum heterodyne detection since the
detector radius is 72% of the diffraction-limited focal spot radius.
The nominal laser spot diameter on the ground is 10.5 cm, which corre-
sponds to a power density of 115 mW/cm².

The dwell time of the laser on a particular pixel on the ground
is τ = 0.51 μsec, and the dwell-time bandwidth is B = $1/\tau$ = 2 MHz. The
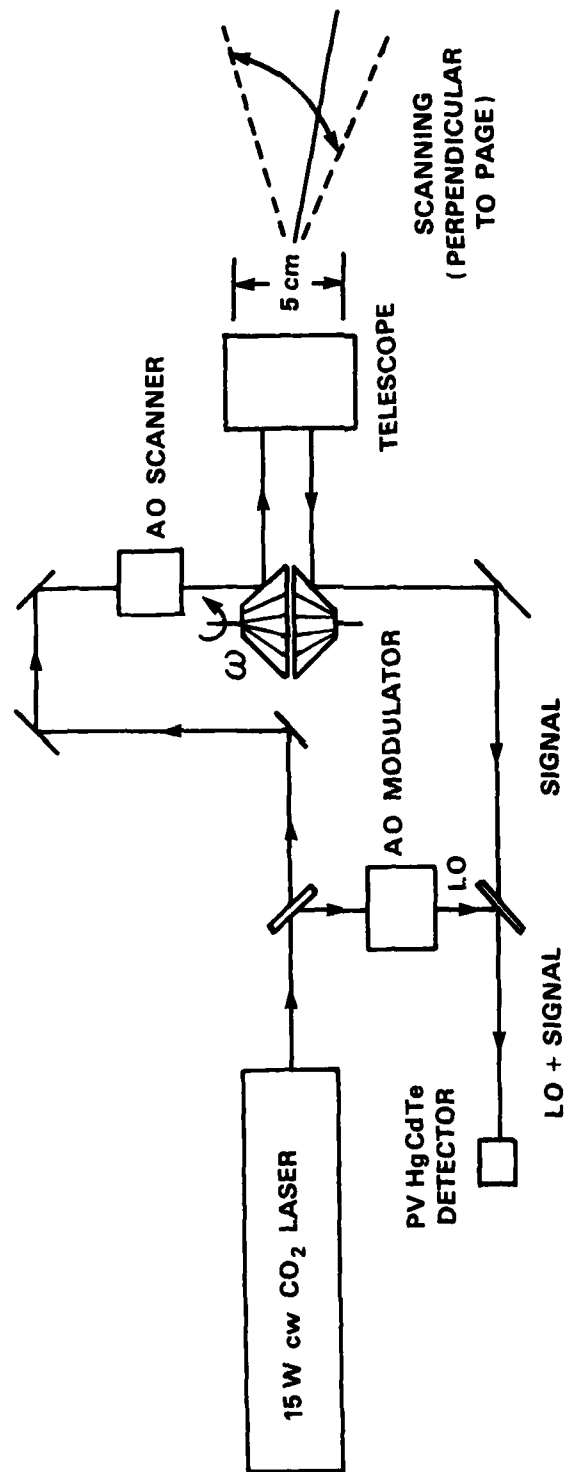
Figure 5.1

HETERODYNE - DETECTION RMD CO_2 LASER RADAR

polygonal mirrors rotate at 4800 rpm which gives the desired angular
scanning rate of 503.5 rad/sec. The rms Doppler broadening due to the
moving mirrors (see Appendix H) is $\Delta \nu = 700$ kHz.

Assuming that the system is photon-noise limited, and that
there is no depolarization, the power signal-to-noise ratio of the
heterodyne sensor is

$$SNR = \eta P_s / E_\lambda B = 1.86 (10^{13})\ P_s$$

where P_s is the signal power received in Watts, and the bandwidth of
the system is taken to be the 2 MHz dwell-time bandwidth. For a dif-
fuse background with a 10% albedo the received signal power is 62.5 nW,
which gives a SNR of over (10^6). The signal-to-noise due to speckle is
still however one.

5.3   Incoherent Sensor Design

The direct-detection RMD sensor, shown in Figure 5.2, uses a
pulsed CO_2 laser and a 1024-element linear array IR photodetector. The
detector is a hybrid photovoltaic focal-plane array of mercury cadmium
telluride. Unlike the heterodyne-detection design separate transmit
and receive optics are used. The 5 cm diameter receiver lens has a
focal length of 10 cm, (i.e., f/2 optics). The length of the linear
detector array is 2.6 cm and the elements are 20 μm square with 5 μm
spacing. The focal plane array is located behind a spectral filter
which has a 2 μm bandwidth. Both the array and the filter are cooled
to 77 K, as shown in Figure 5.3, with the cooled enclosure having a
cone angle of $\theta = 20°$.
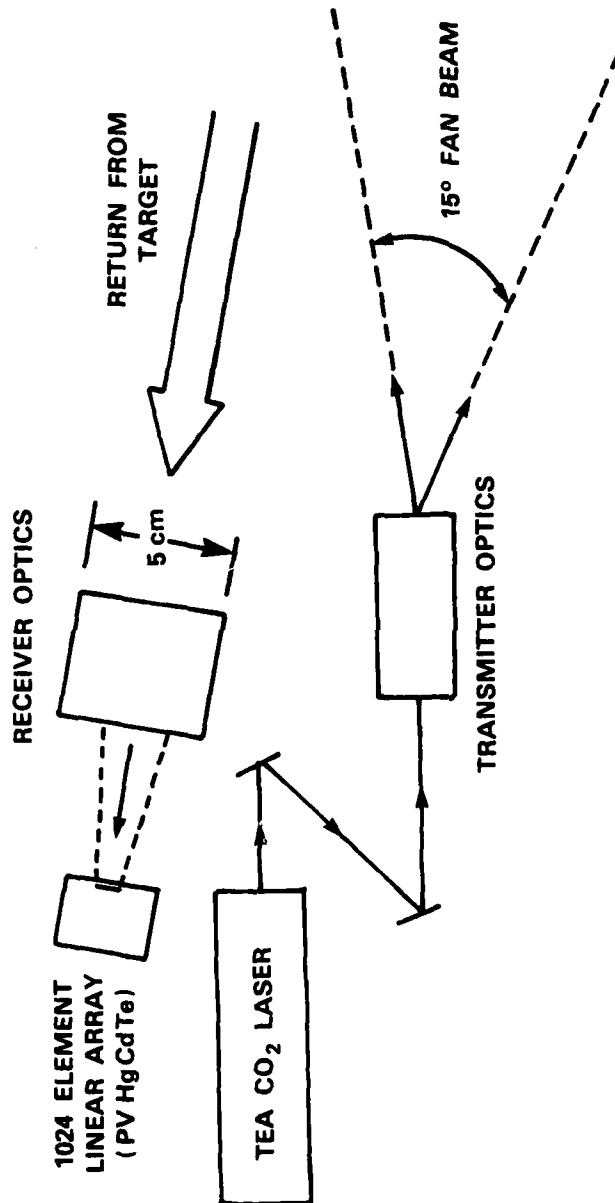
Figure 5.2

DIRECT-DETECTION RMD CO_2 LASER RADAR

VACUUM VESSEL

EXTERNAL
WINDOW

20°

2 μm
FILTER

HgCdTe
ARRAY

LIQUID
NITROGEN (77 K)
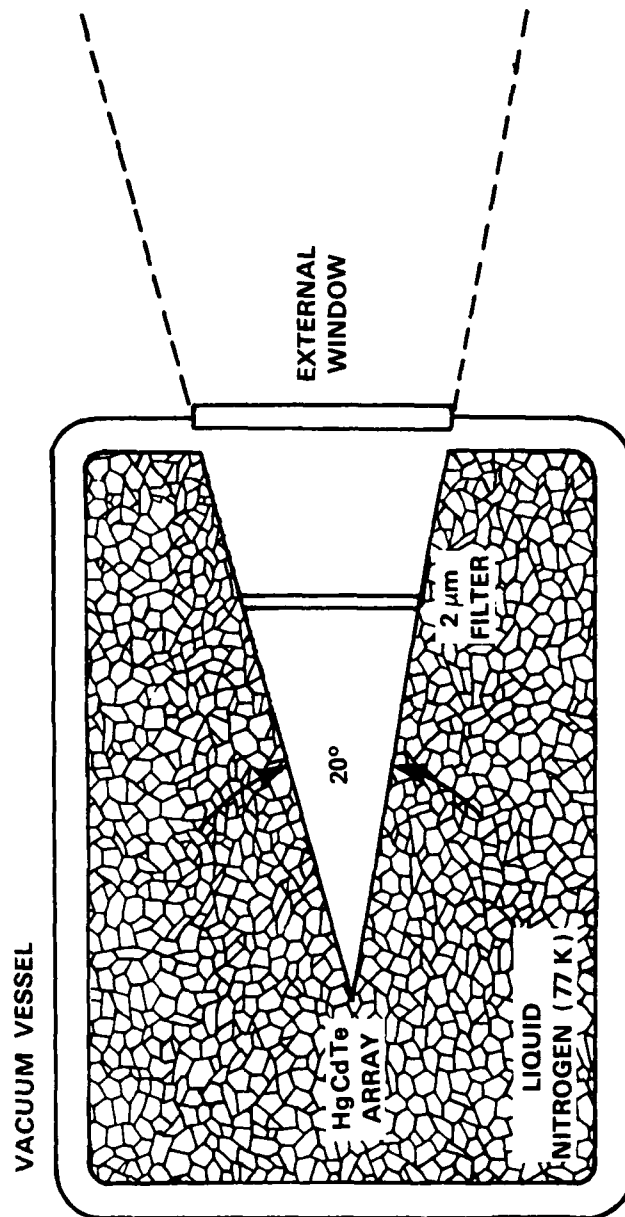
Figure 5.3

COOLING OF DETECTOR ARRAY AND SPECTRAL FILTER

The limiting noise of the direct detection is assumed to be the 300 K thermal background photon noise. The background power on an individual element of the focal-plane array is 0.61 nW. Taking this to be the noise-equivalent-power (NEP) means the detectivity of the detector element, for a bandwidth of B = 2 MHz, is

$$D^* = \sqrt{A_d B}/NEP$$
$$= 4.63(10^9) \text{ cm Hz}^{\frac{1}{2}}W.$$

The power that each element of the array measures for a target with an albebo of 10% is $P_s = 6.1(10^{-12}) P_T$, where P_T is the transmitted laser power measured in Watts. The signal-to-noise ratio is therefore $SNR = P_s/NEP = 0.01 P_T$.

The laser used in the RMD direct-detection sensor is a grating-tuned TEA (transverse electrical discharge, atmospheric pressure) CO_2 laser with a pulse repetition frequency of 1.923 kHz, a pulse energy of 10 mJ, and a pulse width of 1 μs. The peak pulse power of 10 kW gives the direct-detection CO_2 laser radar a maximum SNR of the order of 100. The output of the TEA CO_2 laser is passed through anamorphic optics to give a 15 degree-wide fan beam. The footprint of this beam on the ground is 26.3 m wide by 10 cm long. The TEM_{∞} output of the direct-detection laser is modified by using a phase plate in the near field to give a flat intensity distribution in the far field. Without this modification the Gaussian profile across the swath width would result in a corresponding intensity distribution in the returned signals. The beam intensity on the ground is approximately the same for both the heterodyne and direct laser radars.

5.4   Design Summary

The characteristics of the two RMD CO_2 laser radars are summarized in Table 5.2. Both systems operate at 10.6 μm, have an angular resolution of 0.256 mrad, and a total field-of-view of 15 degrees. The signal-to-noise ratios quoted are the maximum power SNRs which do not consider speckle noise.

TABLE 5.2

SUMMARY OF THE TWO RMD SENSOR DESIGNS

	Heterodyne System	Direct System
CO_2 Laser	cw, 15 W, rf waveguide	pulsed, 10 kW, TEA
Detector	single PV HgCdTe 0.1 mm radius	linear PV HgCdTe array 1024 elements, 20 μm
Scanning	line-scan	pushbroom
Receiver Optics	5 cm, f/11	5 cm, f/2
SNR	10^6	10^2

6.   EXPECTED RMD RESULTS

6.1   Model Scatterable Minefield

By creating a simple model of a scatterable minefield, the type of data expected from the two RMD sensor designs can be generated. This model uses several major assumptions, and does not attempt to accurately predict the complexity of the returns which would occur in an actual operational situation. The intent of the model is to indicate the typical sorts of signals which may be encountered by the airborne CO_2 laser radars, particularly the noise component due to speckle. To this end, the following assumptions have been made:

(1)   The ground is taken to be a flat, Lambertian surface. The albedo (hemispherical reflectance) of grass is assumed to be 3% while that of asphalt is 10%.

(2)   The atmospheric attenuation is 1.5 km^{-1} and there is no turbulence.

(3)   The RMD aircraft is a perfectly stable platform which is flying at a constant altitude of 100 m.

(4)   The scatterable mines are all laying flat on ground.

(5)   The reflectance of each mine is taken to be that of Figure 3.4. This reflectance is similar to that of a dry military green paint. The retro-reflectivity has an exponential fall-off with the incident angle for angles $\theta < 10°$, and is given by

$$R = 10.0 \exp[-0.558\theta] sr^{-1}.$$

The flight-path of the RMD aircraft and the distribution of the mines is given in Figure 6.1. The scan-line shown in the figure crosses
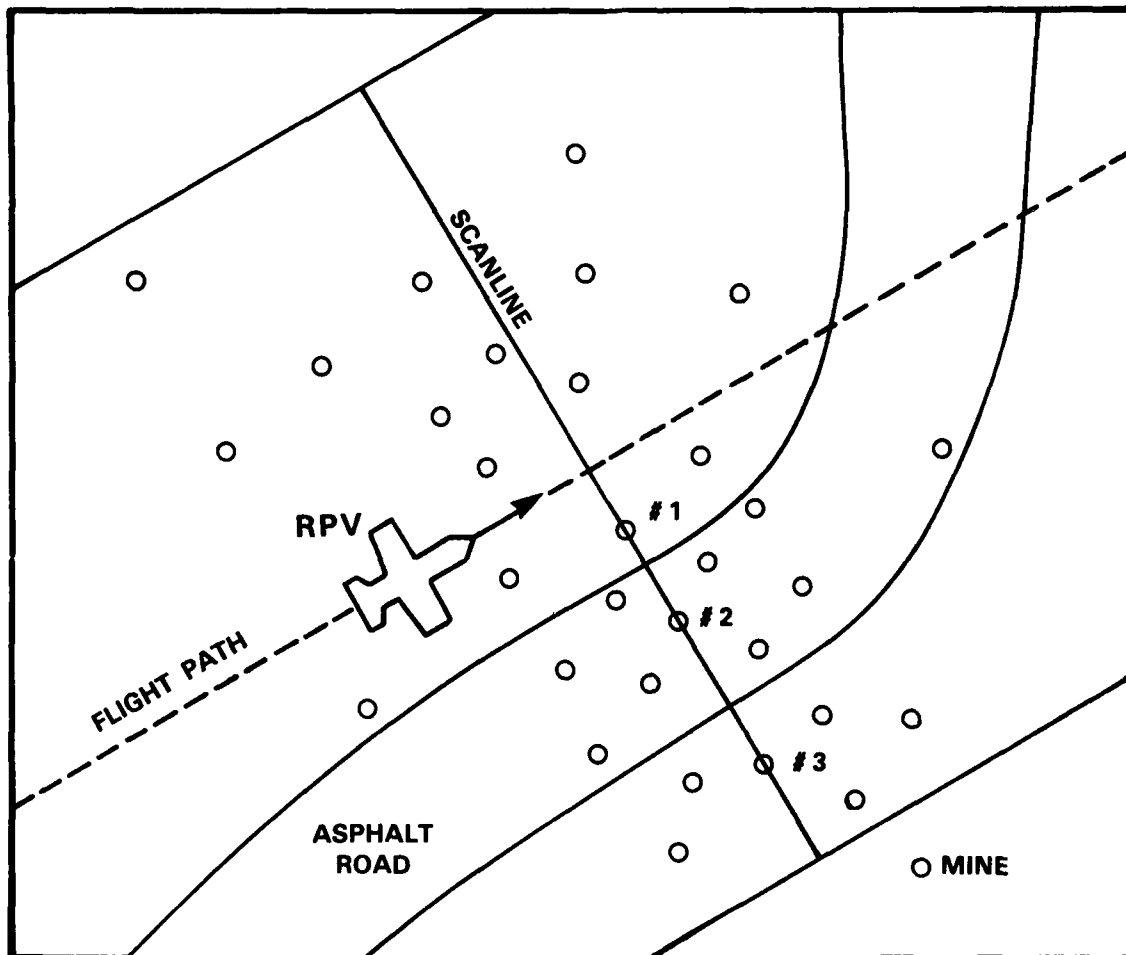
Figure 6.1

MODEL OF A SCATTERABLE MINEFIELD

three mines which are located 2 m, 5 m and 10 m from nadir. One of the mines is on the asphalt road while the remaining two scatterable mines are lying on the grass. The three mines on the scan-line are labelled as numbers 1, 2 and 3 respectively.

6.2   Coherent Detection Results

Figure 6.2 gives the signal which would be obtained using the heterodyne detection CO_2 laser radar. The figure shows the half of the scanline which intercepts the three scatterable mines. The grass and asphalt backgrounds are characterized by Rayleigh distributions with means of 14 nW and 46 nW. The speckle effects are quite pronounced, with the speckle maximas being comparable to the returns from mines #2 and #3.

6.3   Incoherent Detection Results

The signal from the direct detection sensor is shown in Figure 6.3. In this case the background speckle noise is approximately Gaussian, with the grass having a mean of 13.6 nW and a standard deviation of 3.4 nW, and the road having a mean of 45 nW and a deviation of 11 nW. Unlike the heterodyne system, all three mines can be readily distinguished above the local background noise.

Note that the returns from the mines and the mean background signals are only a factor of 1.024 lower than those for the heterodyne detection system. The 10 kW peak power of the direct-detection system's transmitter combined with its 1024 element array make it equivalent, in terms of power, to the 10 W heterodyne laser radar. The direct-detection scheme, however, has far less speckle noise than the heterodyne detection design.
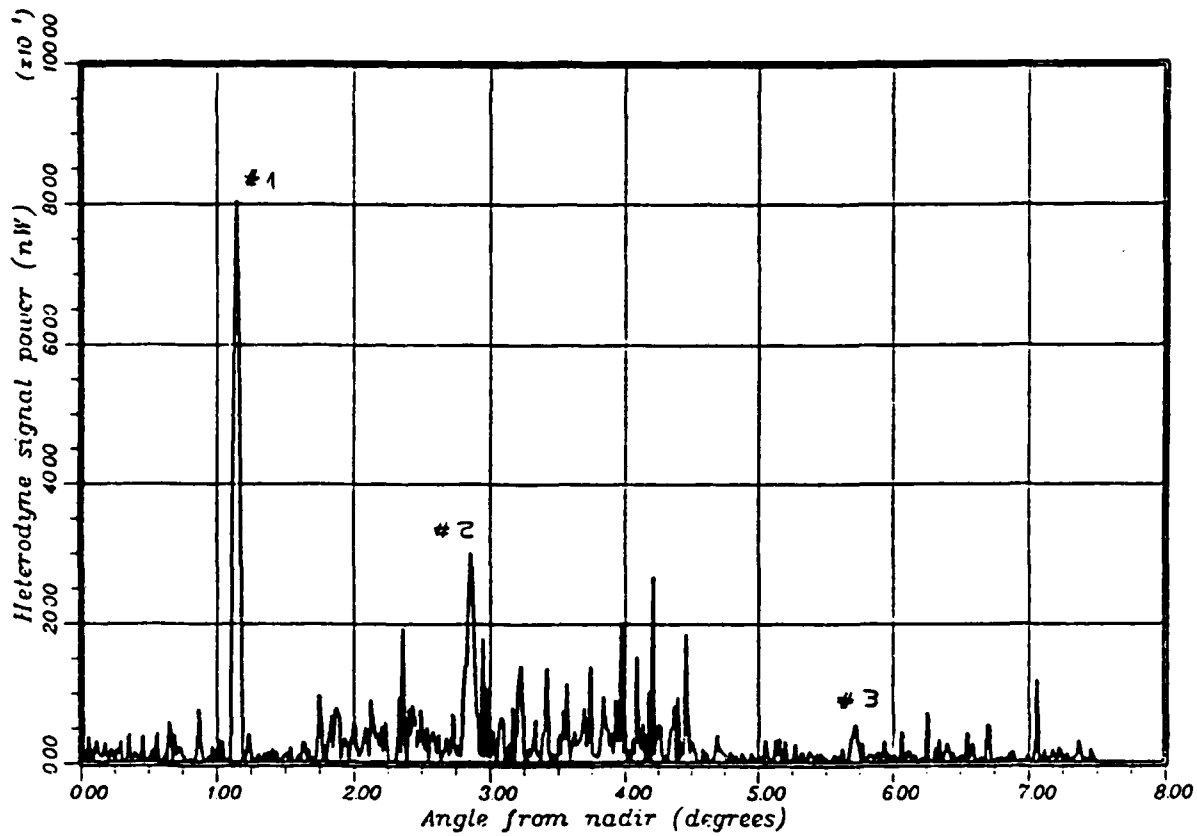
Figure 6.2: Results with the Heterodyne-Detection RMD System
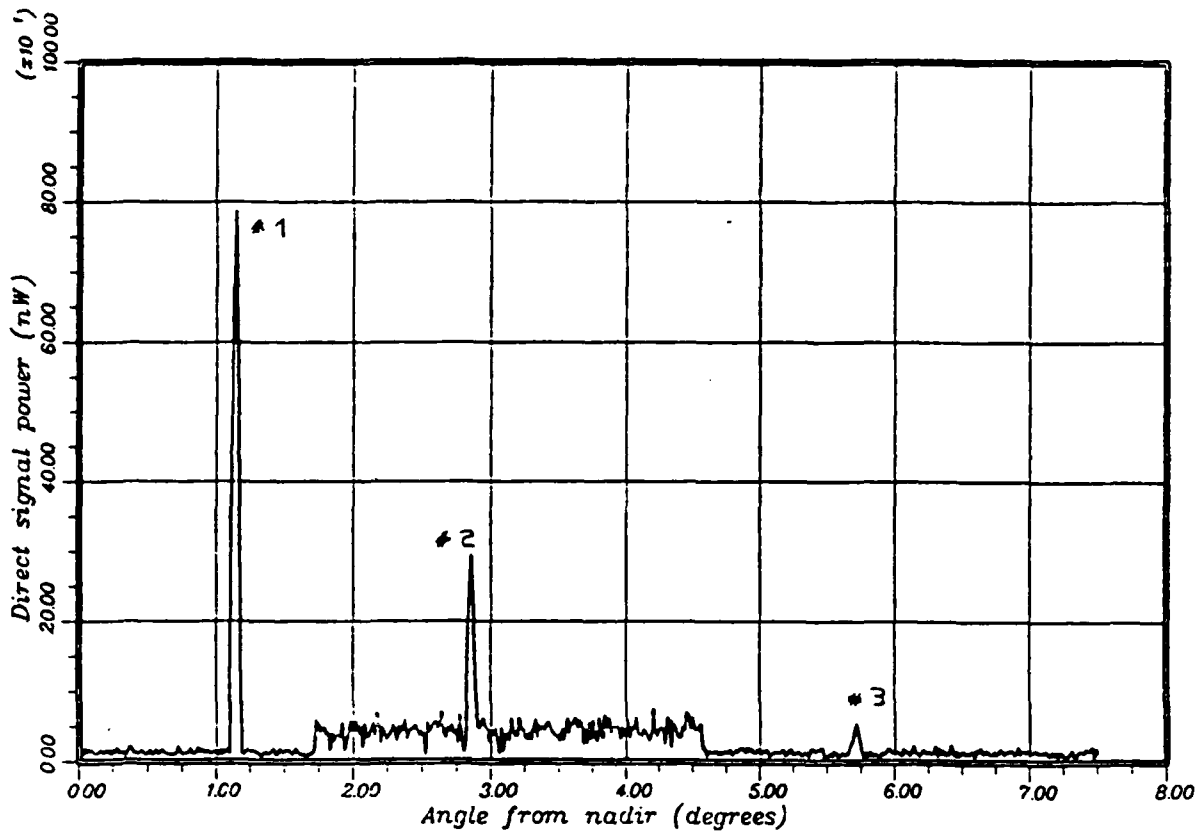
Figure 6.3: Results with the Direct-Detection RMD System

7.   COUNTERMEASURES

7.1   Active and Passive Countermeasures

Any attempt to design a possible RMD system must consider
likely countermeasures, if for no other reason than to postulate rea-
sonable limits on the system's capabilities. The entire concept for
RMD rests on the assumption that images of a minefield can be obtained
and that mines will be sufficiently distinct from other elements of the
image to be identified. There are both active and passive counter-
measures just as there are active and passive RMD techniques. Active
measures would include standard approaches such as attacking the air-
craft or ground station and the jamming of data links, in addition to
optical methods like blinding the infrared sensors. In terms of pas-
sive measures there are two obvious directions to be investigated.
Firstly, one must consider that the enemy would try to make their mines
as indistinguishable as possible. Mines can be made more difficult to
detect by utilizing anti-reflective coatings and by modifying their
shapes. Secondly, decoys could be developed which would appear to be
actual mines when imaged by the RMD system.

7.2   Mine Paints and Surface Texture

The introduction of CO_2 laser rangefinders and target designa-
tors to the modern battlefield has resulted in the use of specialized
IR-absorbing coatings on military vehicles. These paints have very low
reflectivity in the thermal infrared. As new imaging CO_2 laser radars
are developed it can be assumed that the use of such coatings will
increase. In addition to painting mines with an anti-reflective
material their detectability can be reduced by ensuring that their sur-
faces are rough rather than smooth. Diffuse targets are much harder to
identify, especially for an RMD system where the ability to deal effec-
tively with speckle is very limited.

The trade-off between reflectivity and emissivity has important ramifications in terms of both RMD design and possible RMD counter-measures. For optically-thick targets the wavelength-dependent reflectivity, ρ_λ, and emissivity, ϵ_λ, are related through $\rho_\lambda + \epsilon_\lambda = 1$. A mine coated with a low emissivity paint would reflect the IR beam effectively and would be relatively easy to detect with an active IR system. Conversely a coating of high-emissivity paint would tend to absorb more ambient radiation and become somewhat warmer than its surroundings, making the mine detectable by a passive thermal IR system. Not withstanding specialized coatings, the emissivity of common paints can vary significantly in the 8 μm to 14 μm IR band yet be very similar at visible wavelengths. For example, two naval paints, both grey in color, have a factor of two difference in IR emissivities, with one measured[1] at $\epsilon_{10.6\mu m} = 0.86$ and the other at $\epsilon_{10.6\mu m} = 0.44$.

The whole question of mine camouflage will have to be re-addressed if and when RMD systems, operating in the thermal IR or at other wavelengths beyond the visible range, come into service. No longer will it be sufficient to simply consider the appearance of mines to the human eye or to conventional aerial photography.

7.3   Mine Geometry and Orientation

The shape of any scatterable mine is an important factor in determining its detectability by active remote minefield detection. An RMD system relies on the specular reflectivity of the mines being concentrated in a relatively small cone angle of acceptance. Any surface which is oriented such that the reflection is directed at an angle greater than the RMD sensor's acceptance angle will be, for all intents and purposes, invisible to the system. In the case of the CO_2 laser radar designs proposed here, mines with surfaces inclined at more than 10 degrees will be very difficult, if not impossible, to detect.

Just as importantly, the orientation of the mines as they lie on the ground also affects whether they are visible to the airborne RMD sensors. Even if the mines themselves are flat they may be resting at angles to the ground which are sufficient to direct the reflections away from the sensors' cone angles. Mine designs could increase the probability that mines do not "lay flat".

7.4   Scatterable Decoy Minefields

Decoy minefields could be readily laid using highly reflective, mine-sized targets. These deccys would have the same diameter as the actual mines but could be considerably thinner. An artillery shell or rocket could disperse hundreds or thousands of these decoys. Differences in the patterns of actual scatterable minefields and those of decoys may be used as means of discrimination but this increases the complexity of the image processing algorithms.

8.   CONCLUSIONS

8.1   Coherent or Direct Detection

High-resolution CO_2 laser radars, using either heterodyne or direct detection, have shown significant potential for detecting scatterable mines in a simple, well-defined natural environment. Mines which are predominantly specular at 10.6 μm may be found with little difficulty provided they are oriented such that a significant part of the reflected signal is directed towards the RMD aircraft. Given that the angular orientations of the mines in an actual minefield will likely be randomly distributed around nadir, there is a high probability that an active IR sensor will detect a number of these specular

mines. Any CO_2 laser radar will have substantial difficulty in distin-
guishing diffuse mines from typical natural backgrounds because of
speckle effects. Speckle is much more severe in heterodyne systems
which results in a higher false-alarm rate than that of systems using
direct detection.

Direct detection is superior to heterodyne detection for CO_2
laser radars which are being used solely for the purpose of remote
minefield detection. The larger speckle noise of a heterodyne detec-
tion scheme is too serious to justify its use in a situation where the
targets, namely mines, are all stationary. Coherent laser radars have
tremendous capability in other applications where their ability to
simultaneously provide range, velocity and intensity information is
invaluable. The decision of whether or not heterodyne detection is
appropriate may ultimately depend on military requirements. These may
necessitate active IR systems which can function in a wide variety of
roles and the cost and complexity of high-resolution airborne CO_2 laser
radars could make them impractical for dedicated remote minefield
detection. Infrared imaging sensors can be used to detect targets
other than mines, and an extended multi-function capability is compara-
tively easy to achieve, especially with heterodyne detection. A pod-
mounted imaging CO_2 laser radar could be fitted to any tactical air-
frame and use in a number of roles from RMD to ground attack. The
0.26 mrad angular resolution represents a pixel size of 50 cm from an
altitude of 2000 m, which may be sufficient to detect, identify, track
and target vehicles on the ground.

8.2   Combined Active and Passive System

Both active and passive IR systems have limitations in terms of
their application to RMD. As discussed in Section 1.2 passive RMD is

greatly influenced by environmental factors and the diurnal cycle and active RMD can be countered using the techniques of Section 7. A system which simultaneously makes active and passive thermal IR measurements would be vastly superior to either of the two individual methods. The optics, HgCdTe photodetectors and amplifier electronics of a direct-detection CO_2 laser radar are entirely compatible with passive thermal IR scanners. In fact a pulsed direct-detection CO_2 laser radar is an active system during the laser pulses and a passive thermal IR system between pulses.

8.3   Relevant New Technology

High-performance, airborne, imaging CO_2 laser radars have become more feasible due to recent developments in many areas of technology, and an understanding of the current state-of-the-art in these various fields is important. There are a number of critical technologies which will determine the feasibility, cost and performance of an RMD system based on CO_2 laser radar. Improved diamond-turning has lead to better eccentric-pupil optics and holographic beam-shaping has allowed efficient heterodyne detection with detector arrays. The development of large, two-dimensional HgCdTe focal-plane arrays has been particularly significant.

These advances have a great impact on CO_2 laser radar design and consequently on the problem of RMD itself. The final RMD system may in fact use scanned, two-dimensional focal-plane arrays of high-temperature HgCdTe[42], and processing techniques such as time-delay and integration (TDI).

8.4   Future Directions

The successful application of CO_2 laser radars to RMD requires detailed knowledge on the reflectance characteristics of mines and the environments in which they are deployed. A large amount of data exists on the reflectivity of different materials at 10.6 μm but very little is available on actual mines. Of equal importance is knowledge of the reflectance of military paints including the anti-IR reflective types which, if not currently in use, might eventually be applied as a countermeasure. Experiments should investigate different mine shapes and textures, the effects of water or dirt on mine surfaces, and the 10.6 μm reflectance and statistical distribution of various materials within the natural environment.

Given that a CO_2 laser radar will be imaging stationary targets on the ground, investigations should be focussed on direct detection. Of particular significance are speckle-reduction techniques. The statistical characteristics of speckle and aperture-averaging effects must be examined in much greater detail.

9.   REFERENCES

1.   W.G. Driscoll and W. Vaughan (eds.), HANDBOOK OF OPTICS,
      McGraw-Hill, New York, 1978.

2.   R.C. Harney, "Military Applications of Coherent Infrared
      Radar", SPIE Volume 300, Physics and Technology of Coherent
      Infrared Radar, pp. 2, 1981.

3.   M.J. Kavaya, R.T. Menzies, D.A. Haner, et al., "Target Reflec-
      tance Measurements for Calibration of Lidar Atmospheric Back-
      scatter Data", Appl. Opt., 22, (17), pp. 2619, 1983.

4.   T.H. Courtenay, J.F. Boulter and H. Henshall, "Active Imaging
      with a TEA CO_2 Laser", Infrared Physics, 16, pp. 95, 1976.

5.   H. Henshall, P. St. Pierre and T.H. Courtenay, "Measurements of
      the Reflectance of Materials at 10.6 Microns using a TEA CO_2
      Ladar", DREV Report 4051, June 1976, UNCLASSIFIED.

6.   J.M. Cruickshank, "Transversely Excited Atmospheric CO_2 Laser
      Radar with Heterodyne Detection", Appl. Opt., 18, (3), pp. 290,
      1979.

7.   J.M. Cruickshank, V. Larochelle, P. Pace, et al., "Investiga-
      tion of a CO_2 Laser Rangefinder for the Leopard C1 Tank: Final
      Report", DREV Report 4468, September 1987, UNCLASSIFIED.

8.   R.A. Brandewie and W.C. Davis, "Parametric Study of a
      10.6 Micron Laser Radar", Appl. Opt., 11, (7), pp. 1526, 1972.

9.   W. Alexander, D.L. Clark and C.A. Stewart, "A CO_2 Laser Radar
        Configured for Doppler Imaging", SPIE Volume 806, Active Infra-
        red Systems and Technology, pp. 102, 1987, and "Coherent Opti-
        cal Radar", Opt. Eng., 27, (1), pp. 11, 1988.

10.   D. Letalick, I. Renhorn and O. Steinvall, "Measured Signal
        Amplitude Distributions for a Coherent FM-cw CO_2 Laser Radar",
        Appl. Opt., 25, (21), pp. 3927, 1986.

11.   O. Steinvall, G. Bolander, K. Gullberg, et al., "Experimental
        Studies with a Coherent CO_2 Laser Radar", SPIE Volume 300,
        Physics and Technology of Coherent Infrared Radar, pp. 100,
        1981.

12.   I. Renhorn, O. Steinvall, D. Letalick, et al., "Performance
        Study of a Coherent Laser Radar", SPIE Volume 415, Coherent
        Infrared Radar Systems and Applications II, pp. 39, 1983.

13.   R.M. Hardesty, R.J. Keeler, M.J. Post and R.A. Richter, "Char-
        acteristics of Coherent Lidar Returns from Calibration Targets
        and Aerosols", Appl. Opt., 20, (21), pp. 3763, 1981.

14.   D.K. Killinger and N. Menyuk, "Remote Probing of the Atmosphere
        using a CO_2 DIAL System", IEEE J. Quantum Electr., 17, (9),
        pp. 1917, 1981.

15.   D.K. Killinger, N. Menyuk and W.E. DeFeo, "Experimental Compar-
        ision of Heterodyne and Direct Detection for Pulsed Differen-
        tial Absorption CO_2 Lidar", Appl. Opt., 22, (5), pp. 682,
        1983.

16.   R.C. Harney and R.J. Hull, "Compact Infrared Radar Technology",
        SPIE Volume 227, CO_2 Laser Devices and Applications, pp. 162,
        1980.

17.   D.R. Sullivan, R.C. Harney and J.S. Martin, "Real-Time Quasi-
        Three-Dimensional Display of Infrared Radar Images", SPIE Pro-
        ceedings, Volume 180, Real-time Signal Processing II, pp. 56,
        1979.

18.   R.J. Keyes, "Heterodyne and Nonheterodyne Laser Transceivers",
        Rev. Sci. Instrum., 57, (4), pp. 519, 1986.

19.   R.J. Hull and S. Marcus, "A Tactical 10.6 µm Imaging Radar",
        IEEE Nat. Aero. Electr. Conf., Volume II, pp. 662, 1978.

20.   D.J. Wilson, R. Foord and G.D.J. Constant, "Operation of an
        Intermediate Temperature Detector in a 10.6 µm Heterodyne
        Rangefinder", SPIE Volume 663, Laser Radar Technology and
        Applications, pp. 155, 1986.

21.   M.J. Post, R.A. Richter, R.M. Hardesty, et al., "National
        Oceanic and Atmospheric Administration's (NOAA) Pulsed,
        Coherent, Infrared Doppler Lidar - Characteristics and Data",
        SPIE Volume 300, Physics and Technology of Coherent Infrared
        Radar, pp. 60, 1981.

22.   R.M. Hardesty, T.R. Lawrence, R.A. Richter, et al., "Ground-
        Based Coherent Lidar Measurement of Tropospheric and Strato-
        spheric Parameters", SPIE Volume 415, Coherent Infrared Radar
        Systems and Applications II, pp. 85, 1983.

23.   J.Y. Wang, B.J. Bartholomew, M.L. Streiff, et al., "Field Tests and Signature Analysis of an Imaging CO_2 Laser Radar", SPIE Volume 415, Coherent Infrared Radar Systems and Applications II, pp. 21, 1983.

24.   J.L. Bufton, T. Itabe and D.A. Grolemund, "Dual-Wavelength Correlation Measurements with an Airborne Pulsed Carbon Dioxide Lidar System", Opt. Lett., 7, (12), pp. 584, 1982.

25.   A.B. Kahle, M.S. Shumate and D.B. Nash, "Active Airborne Infrared Laser System for Identification of Surface Rocks and Minerals", Geo. Res. Lett., 11, (11), pp. 1149, 1984.

26.   W. Wiesemann, R. Beck, W. Englisch and K. Gurs, "In-Flight Test of a Continuous Laser Remote Sensing System", Appl. Phys., 15, pp. 257, 1978.

27.   W. Wiesemann, F. Lehmann and C. Werner, "Probing of the Earth's Surface and the Atmosphere with an Airborne Laser Spectrometer", Infrared Physics, 25, (1/2), pp. 467, 1985.

28.   R.L. Del Boca and R.J. Mongeon, "Multifunction CO_2 Laser Radar Technology", SPIE Volume 300, Physics and Technology of Coherent Infrared Radar, pp. 18, 1981, and "Multifunction CO_2 Heterodyning Laser Radar for Low Level Tactical Applications", IEEE Nat. Aero. Electr. Conf., Volume III, pp. 1079, 1979.

29.   B. Stephan and R. Metivier, "Flight Evaluation Trials of a Heterodyne CO_2 Laser Radar", SPIE Volume 806, Active Infrared Systems and Technology, pp. 110, 1987.

30.   R.W. Frey, R.C. Harney and C.R. Layne, "Laser Imaging Radar
       Sensor (LIRS)", SPIE Volume 415, Coherent Infrared Radar
       Systems and Applications II, pp. 2, 1983.

31.   J.M. Vaughan, D.W. Brown, P.H. Davis, et al., "Atmospheric
       Backscatter at 10.6 μm; A Compendium of Measurements made Out-
       side the United Kingdom by the Airborne LATAS Coherent Laser
       Radar Velocimeter", RSRE Report 87002, May 1987, UNCLASSIFIED.

32.   J.E. Eberhardt, A.A. Green, J.G. Haub, R.J.P. Lyon and
       A.W. Pryor, "Mid-Infrared Remote Sensing Systems and Their
       Application to Lithologic Mapping", IEEE Trans. Geo. Rem.
       Sens., GE-25, (2), pp 230, 1987.

33.   D.E. Watson, et al., "MICOS I", Volumes I and II, Ford Aero-
       space, Report for US Air Force Aeronautical Laboratories,
       AFWAL-TR-84-1180, October 1984, UNCLASSIFIED.

34.   R.C. Harney, "Design Considerations for the Infrared Airborne
       Radar (IRAR) MIT Subsystem", MIT Lincoln Laboratory, Project
       Report TST-26, July 1980, UNCLASSIFIED.

35.   R.C. Harney, "Conceptual Design of a Multifunction Infrared
       Radar for the Tactical Ground Attack Scenario", MIT Lincoln
       Laboratory, Project Report TST-25, August 1978, UNCLASSIFIED.

36.   R.J. Becherer and W.B. Veldkamp, "Holographic Beam Shaping for
       Optical Heterodyne Arrays in Laser Radars", SPIE Volume 300,
       Physics and Technology of Coherent Infrared Radar, pp. 185,
       1981.

37.   M.C. Teich, "Infrared Heterodyne Detection", Proc. IEEE, 56,
        (1), pp. 37, 1968.

38.   S.F. Jacobs, "Optical Heterodyne (Coherent) Detection", Am. J.
        Phys., 56, (3), pp. 235, 1988.

39.   R.J. Keyes, "Heterodyne and Nonheterodyne Laser Transceivers",
        Rev. Sci, Instrum., 57, (4), pp. 519, 1986.

40.   A.E. Siegman, "The Antenna Properties of Optical Heterodyne
        Receivers", Proc. IEEE, 54, (10), pp. 1350, 1966.

41.   H. Henshall, "An Infrared Evaluation of Two Naval Paints", DREV
        Report 4136, August 1979, UNCLASSIFIED.

42.   M. Grudzien and W. Galus, "High Temperature HgCdTe Detectors
        for CO_2 - Laser Beam Control and Heterodyne Detection", SPIE
        Volume 663, Laser Radar Technology and Applications, pp. 166,
        1986.

43.   J.C. Dainty, LASER SPECKLE AND RELATED PHENOMENA, Topics in
        Applied Physics, Springer-Verlag, 1975.

44.   J.W. Goodman, "Statistical Properties of Laser Speckle Pat-
        terns", in LASER SPECKLE AND RELATED PHENOMENA, Topics in
        Applied Physics, Volume 9, Springer-Verlag, 1975.

45.   J.W. Goodman, "Some Fundamental Properties of Speckle", J. Opt.
        Soc. Am., 66, (11), pp. 1145, 1976.

46.   R. Balcerak, J.F. Gibson, W.A. Gutierrez and J.H. Pollard,
        "Evolution of a New Semiconductor Product: Mercury Cadmium
        Telluride Focal Plane Arrays", Opt. Eng., 26, (3), pp. 191,
        1987.

47.   M.A. Keenan, I.M. Baker, J.E. Parsons, et al., "Advances in
        Linear and Two-Dimensional CdHgTe-Si Hybrid Focal Plane
        Arrays", IEE 3rd Intl. Conf., Advanced IR Detectors and
        Systems, pp. 54, 1986.

48.   D.C. O'Shea, ELEMENTS OF MODERN OPTICAL DESIGN, John Wiley and
        Sons, 1985.

49.   R. Anderson and J.W. Bilbro, "Calibration of the Reflectance of
        Hard Targets for a Coherent Doppler Lidar", Appl. Opt., 27,
        (5), pp. 856, 1988.

50.   J.G. Edwards and P.A. Smith, "Properties of Some Diffusers for
        CO_2 Lasers", J. Phys. E: Sci. Instrum., 14, pp. 1326, 1981.

51.   A. Gross, "Polarization of Reflected 10.6 µm Radiation from
        Sublimed Sulfur Targets", Appl. Opt., 22, (19), pp. 3031,
        1983.

52.   H. Henshall and J. Cruickshank, "Reflectance Characteristics of
        Selected Materials for Reference Targets for 10.6 µm Laser
        Radars", Appl. Opt., 27, (13), pp. 2748, 1988.

53.   M. Kronstein, R.J. Kraushaar and R.E. Deacle, "Sulfur as a
        Standard of Reflectance in the Infrared", J. Opt. Soc. Am., 53,
        (4), pp. 458, 1963.

54.   M.J. Post, R.A. Richter, R.J. Keeler, et al., "Calibration of
        Coherent Lidar Targets", Appl. Opt., 19, (16), pp. 2828, 1980.

55.   M.S. Shumate, S. Lundqvist, U. Persson and S.T. Eng, "Differen-
        tial Reflectance of Natural and Man-Made Materials at CO_2 Laser
        Wavelengths", Appl. Opt., 21, (13), pp. 2386, 1982.

56.   R.N. Colwell (ed.), MANUAL OF REMOTE SENSING, Volume I, 2nd
        Edition, American Society of Photogrammetry, 1983.

57.   J.E. Eberhardt, J.G. Haub and A.W. Pryor, "Reflectivity of
        Natural and Powdered Minerals at CO_2 Laser Wavelengths", Appl.
        Opt., 24, (3), pp. 388, 1985.

58.   W.L. Wolfe and ' J. Zissis (eds.), THE INFRARED HANDBOOK, Envi-
        ronmental Rese ch Institute of Michigan, 1985.

59.   M. Abramowitz and I.A. Stegun (eds.), HANDBOOK OF MATHEMATICAL
        FUNCTIONS, pp. 953, 1964.

APPENDIX A

REFLECTION

REFLECTION

The reflectivity of any object may be considered as being some combination of that from a specular reflector with that of a diffuse surface. The diffuse component of the reflectance is dominant for most naturally-occurring materials such as soil and vegetation, and an understanding of the characteristics of an ideal diffuse surface is important.

A perfectly diffuse, or Lambertian, surface is one where the reflected radiance is uniform in all directions, independent of the angle of illumination. If P_T is the incident power, measured in Watts, then the reflected radiance, with units of W/m^2sr, is given by

$$L = \rho P_T/\pi$$

where ρ is the hemispherical reflectance (albedo). The reflectance represents the fraction of the incident radiation reflected into the entire backwards hemisphere, and $0 < \rho < 1$. The scattered intensity is proportional to the cosine of the viewing angle θ, as shown in Figure A1. An ideal Lambertian surface is completely depolarizing, with the reflected radiation being unpolarized regardless of the state of polarization of the incident radiation.

Considering the situation of Figure A2 where a laser radar is imaging a Lambertian surface from a height h through a non-attenuating atmosphere. Assuming that the receiver field-of-view is sufficiently wide to cover the entire illuminated area, the reflected power received by the lidar is
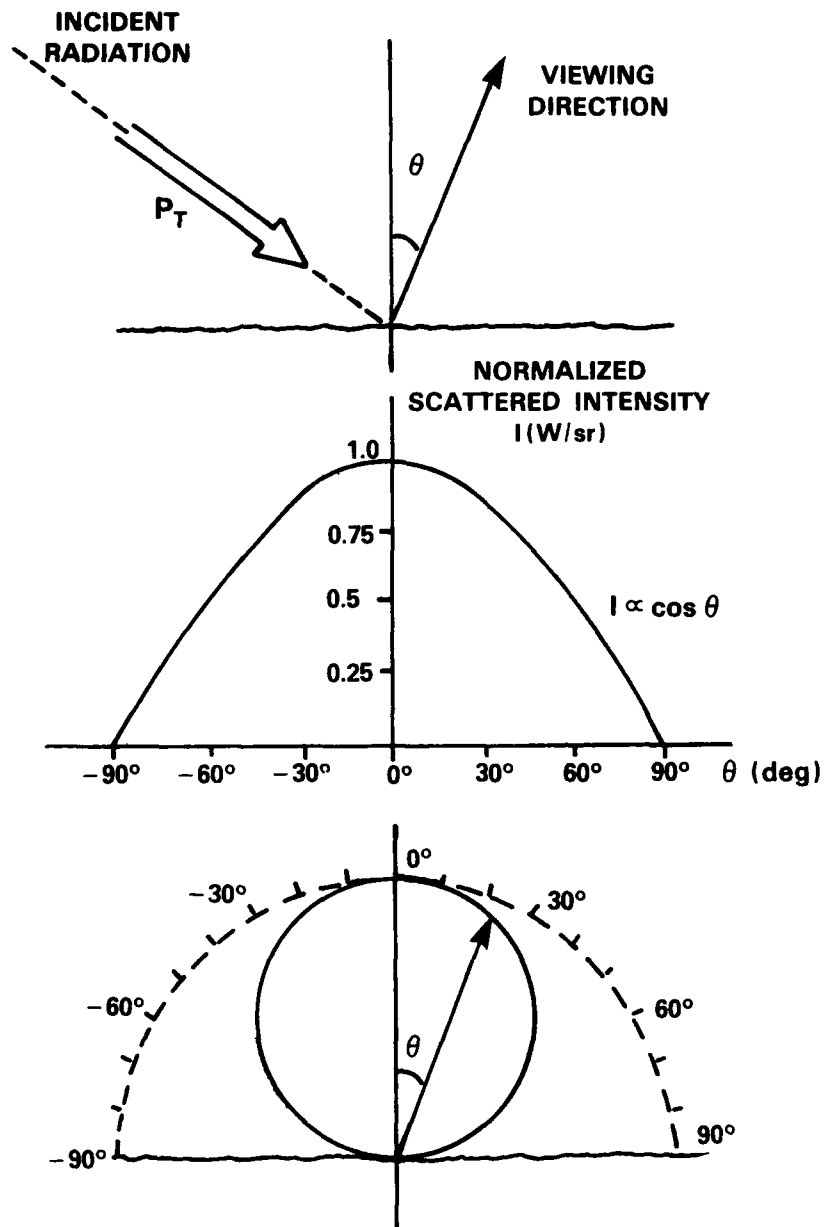
Figure A.1

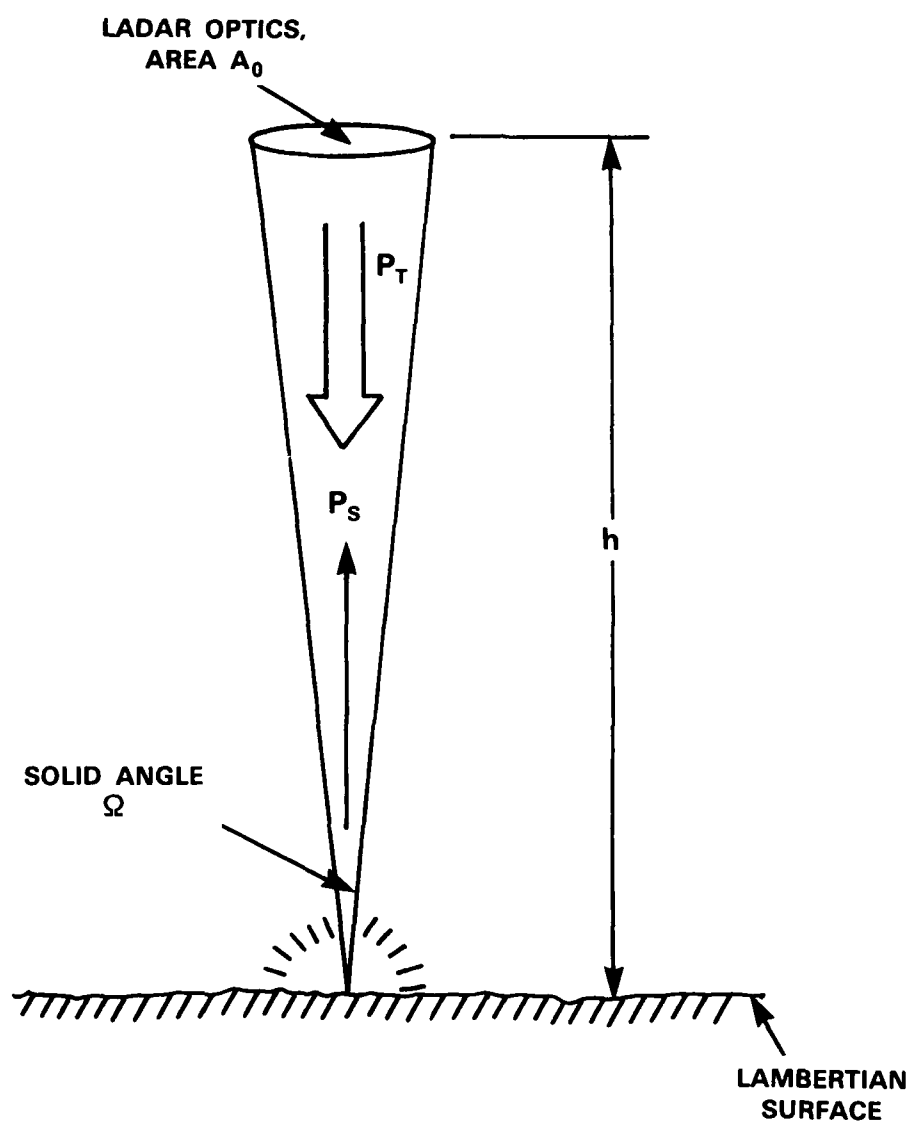SCATTERED INTENSITY FROM A LAMBERTIAN SURFACE

Figure A.2

LADAR IMAGING A LAMBERTIAN SURFACE

$$P_s = \rho \Omega P_T / \pi$$

where $\Omega = A_o/h^2$ is the solid angle subtended by the receiver optics.

The conventional theory of diffuse reflectance is based on classical radiative transfer which involves only the transport of energy, and does not consider interference effects. The relations above hold only in the limit of complete spatial incoherence, which is clearly not the situation when a laser is used as the source of illumination. A coherent beam interacting with a diffuse surface results in the phenomena known as speckle which is the subject of Appendix C. Speckle effects modify the reflectance of a diffuse surface by introducing fine structure in the reflected radiation field, with the power relationships above remaining valid only in terms of statistical averages.

Glints are specular features on an otherwise diffuse target. Normally a glint is the result of specular reflection off a curved surface. A target containing a glint will demonstrate significantly different reflectance characteristics from that of a completely diffuse surface. In general man-made surfaces such as paints, plastics and fabrics tend to be better specular reflectors in the far IR than naturally-occurring surfaces.

Specular reflections are mirror-like reflections from a smooth surface which are described by the Fresnel equations. These equations give the intensity and polarization of the reflected radiation for a specified incident beam. The Fresnel equations utilize the complex refractive index of a material, which is given by,

$$n^* = n - ik$$

where n is the intrinsic refractive index, and k is the absorption
index. The absorption index is related to the intrinsic (Lambert)
absorption coefficient, α, and the wavelength, λ, through

$$k = \alpha\lambda/4\pi.$$

For normal incidence the reflectivity is given by

$$R = [(n-1)^2 + k^2]/[(n+1)^2 + k^2].$$

A metal has a non-zero k which is usually sufficiently large so as to
make R = 1 in the infrared. For example aluminum has n = 31.2 and
k = 104 at 10 μm, which gives a 99% reflectivity. The reflectivity of
a dielectric, with k = 0, is the familiar result

$$R = (n-1)^2/(n+1)^2.$$

Germanium (n = 4) and ZnSe (n = 2.4), which are two of the most common
optical materials used for transmissive optics at 10 μm infrared wave-
lengths, have reflectivities of 36% and 17% respectively. These high
reflectivities are the reason why these materials are almost always
anti-reflection coated.

The IR reflectance spectra of many minerals is often dominated
by a process known as Restrahlen (residual ray) and this is often dis-
cussed when active IR systems are used for geologic mapping. Anomalous
absorption in the mineral is characterized by sharp peaks in the
absorption, and hence reflection spectra, which are due to resonances
with the fundamental vibrational modes. Silicate minerals have strong
restrahlen bands around 10 μm which are associated with Si-O bond-

stretching modes. For restrahlen at a wavelength of 10.6 μm the
absorption coefficient α is of the order of 10^6 m^{-1} and the absorption
index is k = 1.

The relatively simple theory of specular and diffuse reflec-
tion, as outlined above, cannot be used to describe the interaction
between incident radiation and a complicated particulate structure such
as a leaf or a powdered layer. Particulate bodies require the use of
the theory of multiple scattering. Multiple scattering effects are
also very important when one is considering the transmission of a laser
beam through the atmosphere and during reflection from clouds, fog,
smoke or dust. There are a large number of multiple scattering models
for use with solid targets and which approach is the most suitable
depends on the composition, surface features, and subsurface structure
of the object in question.

Changes in the polarization state of light upon its reflection
from a given surface provides an additional means of descrimination.
The level of linear polarization can be described in terms of percent-
age as being

$$P = 100[I_{max} - I_{min}/I_{max} + I_{min}]$$

where I_{max} and I_{min} are the maximum and the minimum intensities of the
light transmitted by a rotatable linear polarizer. Rough surfaces will
depolarize an incident polarized beam to a greater extent than will
smooth specular surfaces. Polarized visible light is frequently used
in the remote sensing of vegetation and the proposed RMD systems use
linearly-polarized far infrared radiation.

Lidar studies of clouds have used depolarization to differenti-
ate between cumulus (water drop) clouds and cirrus (ice crystal)
clouds. The depolarization ratio $b = P_\perp/P_\parallel$ is non-zero when the scat-
tering particles are nonspherical, such as with ice-crystals. $P_\perp$ is
the power measured with polarization perpendicular to the transmitted
radiation and $P_\parallel$ is that measured parallel to the transmitted beam.

APPENDIX B

NOISE IN LASER RADARS

NOISE IN LASER RADARS

There are several factors which contribute to un-correlated noise in lidar systems. The most important of these sources of noise are:

(1)   Atmospheric Turbulence

(2)   Fluctuations in laser pointing angle and mode pattern

(3)   Target-Induced Speckle

(4)   Detection noise.

Problems due to propagation through the atmosphere are less severe at CO_2 laser wavelengths than those associated with visible lasers, however detailed analyses of noise in CO_2 laser radars must include atmospheric effects. Fluctuations in the output direction and mode pattern of the transmitter laser can be reduced by careful design of the laser cavity, and this source of noise will not be discussed any further. The fact that optical radar systems use coherent radiation results in the introduction of noise due to speckle effects. Speckle, which is more serious a problem with heterodyne detection systems than with direct detection systems, is discussed in detail in Appendix C. Detection noise includes all the noise sources associated with the detection process itself, and includes background noise, thermal detector noise and photon shot noise. The latter two types of noise in infrared photodetectors are presented in Appendix E.

Atmospheric Turbulence

Turbulence in the atmosphere affects the transmitted laser beam in a number of ways, among which are distortion, intensity modulation

and beam wander. Measurements of the temporal correlation of pulsed DIAL systems have found that the atmosphere remains temporally coherent for times of the order of 1 to 3 msec. The temporal variations are therefore not a concern in the RMD system, where the return-path transit time is of the order of one μsec. However the spatial inhomogenities in the atmosphere may be significant. Fluctuations in the refractive index of the air lead to deviations of the propagating laser beam. These fluctuations are usually much more important than any fluctuations in absorption which occur during beam travel to the target and as the reflected radiation returns to the aircraft. Scintillation, or beam-intensity modulation, can be described using a log-normal amplitude distribution, the normalized variance of which is given by

$$\sigma^2 = \langle I \rangle^2 / \langle I \rangle^2 - 1 = \exp\{4C_\ell^S(0)\} - 1$$

where $C_\ell^S(0)$ is the spherical-wave log-amplitude variance. The log-normal probability density function for the irradiance, I, at a point within the target area is,

$$P(I) = \frac{1}{2I\sqrt{2\pi C_\ell^S(0)}} \exp[-\{\tfrac{1}{2}\ln(I/\langle I \rangle) + C_\ell^S(0)\}^2 / 2C_\ell^S(0)]$$

where $\langle I \rangle$ is the mean irradiance. The superscript "s" refers to the fact that the spherical-wave assumption is used. The log-amplitude variance is a function of the refractive index structure parameter, C_n^2, which is also referred to as the optical strength of the turbulence;

$$C_\ell^S(0) = 0.56 \ K^{7/6} \int_o^L C_n^2(x) |1 - x/z|^{5/3} x^{5/6} dx$$

where k is the wavenumber, L is the length of the turbulence, x is a range variable, and z is the distance from the turbulent region. C_n^2, which has units of $m^{-2/3}$, has been studied by many researchers, and turbulence is described as being "medium" when $C_n^2 = 10^{-14}$ $m^{-2/3}$. Strong daytime turbulence for a CO_2 laser radar operating at an altitude of 2 km has been found to give a σ^2 of the order of 0.01, and result in a beam wander of 15 cm at 1200 m range.

APPENDIX C

SPECKLE

SPECKLE

The presence of laser-induced speckle[43-45] is one of the most serious problems in any laser radar system and it is particularly severe in lidars which use coherent detection. Speckle, which is referred to as clutter in conventional non-optical radar terminology, is a random, high contrast pattern of light and dark regions resulting from interference effects occurring when a rough surface is illuminated with coherent light. The roughness of the diffuse surface must be of the order of the wavelength of the incident light, and the coherence length of the light must exceed twice the roughness of the diffuser. Although random, the statistics of laser speckle patterns are well described. In the case of a polarized speckle pattern the intensity obeys negative exponential statistics while the phase has a uniform distribution. The amplitude of the field in a speckle pattern has a Rayleigh distribution. A single polarized speckle pattern has an intensity contrast of one, while the contrast of the sum of n independent polarized speckle patterns is $1/\sqrt{n}$. The statistical properties of speckle are discussed in greater detail in the following two section of this appendix.

Intensity

If $\langle I \rangle$ is the mean reflected intensity, then the probability density function describing the speckle intensity is

$$P(I) = 1/\langle I \rangle \exp[-I/\langle I \rangle].$$

As with any other negative exponential distribution both the mean and the variance are equal to $\langle I \rangle$, and the most probable intensity is zero. Note that $\langle I \rangle$ represents the intensity one would measure if incoherent light were used.

Consider the situation where the reflected radiation from the diffuse surface is collected by a lens (diameter D and focal length f) and focused onto a detector. In this case the speckle distribution in the focal plane of the lens is determined by diffraction effects due to the finite lens aperture. To account for the aperture-averaging which occurs when a speckle pattern is imaged onto a detector with a lens the probability density function is taken to be that of a gamma distribution,

$$P(I) = [C/\langle I\rangle]^C I^{C-1}/\Gamma(C)\exp[-IC/\langle I\rangle]$$

where C is the number of independently-varying regions (speckle cells) averaged by the lens aperture, and the variance, σ^2, is $\langle I\rangle/C$. For large values of C the gamma distribution for the intensity approaches a Gaussian distribution.

Direct-detection laser radar systems measure the intensity of the signal radiation so that statistics described above are appropriate. Coherent detection laser radars respond to the amplitude of the signal.

Amplitude

The amplitude of the electric field of a speckle pattern for a purely diffuse surface has a Rayleigh probability distribution,

$$P(E) = E/\sigma^2 \exp[-E^2/2\sigma^2]$$

where the mean amplitude $\langle E\rangle$ is related to the standard deviation σ^2 through

$$\langle E \rangle = \sqrt{\pi/2}\sigma.$$

For a diffuse target with a glint the amplitude has a Rician distribution with

$$P(x) = xI_o(\hat{a}x)\exp[-(x^2 + \hat{a}^2)/2]$$

where $x = E/\sigma^2$, I_o is a modified zero-order Bessel function, and $\hat{a}$ is the amplitude due to the glint. In a heterodyne laser system speckle modulation within the return signal is not averaged unlike a direct-detection system. The signal-to-speckle noise ratio of a heterodyne lidar system is always one, and this fact is one of the major drawbacks of heterodyne detection laser radar.

Fresnel Number

An important parameter for determining the severity of speckle effects on a direct-detection laser radar is the Fresnel number,

$$N_F = a_o b/r\lambda$$

where a_o is the radius of the receiving optics, b is the laser spot radius on the diffuse target, r is the target distance, and λ is the laser wavelength. The number of speckle correlation cells, C, within a given aperture is S_m/S_c where S_m is the effective measurement area and S_c is the correlation area of the speckle pattern. The width of each speckle cell at the receiver aperture is given by

$$s = \lambda r/2b.$$

The average number of speckle cells falling within the aperture is given by $C = [2N_F]^2$ and the uncertainty in the return signal, for direct detection, is of the order of $36/N_F\%$. Note that for a heterodyne system, which is necessarily diffraction-limited, the Fresnel number is $N_F = 1/2$ and there is one speckle in the receiver aperture.

The size of the speckle cells at a detector located at the focus of a lens is $\lambda f/D$. For an f/2 lens (e.g., f = 10 cm and D = 5 cm) the speckle cell size is 20 μm when the wavelength is 10.6 μm. The signal-to-speckle noise ratio for the case of direct detection improves as $\sqrt{C}$ where C is the number of speckles on the detector.

Speckle Reduction

Speckle effects can be reduced by spatial and temporal averaging and by using multiple wavelengths since speckle rapidly decorrelates with changes in the laser wavelength. For N different wavelength measurements the accuracy improves as $\sqrt{N}$.

Many laboratory reflectance studies use a rotating target and signal averaging to remove the effects of speckle from the measurements. For any single measurement with a heterodyne detection system the signal-to-noise ratio due to speckle is always unity.

APPENDIX D

CO$_2$ LASERS

CO_2 LASERS

The far-infrared RMD system uses a carbon dioxide (CO_2) laser as the source of the 10.6 μm radiation. CO_2 lasers can be tuned to give a number of wavelengths ranging from just under 9 μm to above 11.5 μm, with wavelength tuning achieved through the use of intracavity elements such as diffraction gratings or piezoelectrically tunable etalons. Rapidly tunable CO_2 lasers use rotating faceted gratings, or rotating polygon mirrors in conjunction with fixed gratings to achieve tuning times of the order of 1 nsec. However in most laser radar applications the CO_2 laser is operated at a single fixed wavelength.

There are many different types of CO_2 lasers, but the nature of their output infrared beams can be used to classify them into the two broad categories of continuous wave (cw) and pulsed. The output of cw lasers may be amplitude or frequency modulated in order to provide range information. Closed-cycle operation of CO_2 lasers is possible through the use of catalysts, such as platinum/tin oxide, which recombine the carbon monoxide and oxygen formed when carbon dioxide is broken down in the discharge.

Continuous Wave Lasers

These lasers are low-pressure devices with the CO_2 gas being excited by an electrical discharge. This discharge can either radio-frequency (rf) or direct-current (dc), and cw lasers whose sizes are suitable for RMD typically produce a 10 to 50 W output beam. The relatively low power of these cw CO_2 lasers often means that heterodyne detection methods are used. With rf-excited lasers care must be taken to ensure that rf noise is not within the bandwidth of the detector

system. Waveguide lasers are more compact than their conventional counterparts since more efficient use is made of the gain volume. Consequently waveguide CO_2 lasers are frequently used in cw and modulated infrared radar systems, and were developed for coherent airborne systems. The efficiency of cw CO_2 waveguide lasers is in the range of 10 to 15%.

Pulsed Lasers

These CO_2 lasers can be either low-pressure or high-pressure devices. For high-pressure operation pulsed transverse discharges are used, the TEA (transversely-excited, atmospheric) CO_2 laser having been developed at DREV in the early 1970's. The high peak powers of pulsed CO_2 lasers enables them to be used for both direct and heterodyne detection. A typical TEA laser used in optical radar has a pulse repetition frequency (PRF) of 500 Hz. The energy of each pulse is up to 1 J and the pulse length may range from 50 ns to 2 µs. Longer pulses are used in lidars to give Doppler velocity measurements, while shorter pulses give precise range readings. Pulsed outputs can be obtained from low-pressure lasers by either pulsing the discharge itself or by Q-switching a continuous discharge. Pulsed low-pressure CO_2 lasers have substantially smaller peak powers than pulsed high pressure lasers but much higher pulse repetition frequencies are possible. Frequency stability is more difficult to achieve with pulsed lasers than with continuous wave lasers, but stability can be within 1 MHz. Intrapulse chirp rates are of the order of 2 MHz/µs² for short cavity TEA lasers, whereas hybrid cw-TEA configurations have 1 MHz/µs² chirp rates, and long-discharge length TEA lasers can have 0.1 MHz/µs² stability.

Table D.1 gives a summary of the characteristics of a variety of compact CO_2 lasers suitable for use in airborne RMD system. In the case of pulsed lasers the output peak powers are given. The average power in the pulsed mode depends on the specific pulse repetition frequency.

Optical heterodyne detection is possible as a result of the long coherence length and high frequency stability of CO_2 lasers. The temporal coherence length of a given laser is

$$\ell = c/\Delta\upsilon$$

where c is the speed of light and $\Delta\upsilon$ is the spectral linewidth. A TEA CO_2 laser has a linewidth of about 3 GHz, which corresponds to a 10 cm coherence length. This far exceeds the degree of coherence required to create speckle effects when the CO_2 laser radiation is reflected by a diffuse surface.

TABLE D.1

TYPICAL CHARACTERISTICS OF COMPACT CO_2 LASERS

	power	pulse duration (ns)	PRF (kHz)
CONTINUOUS WAVE OUTPUT			
low pressure discharge	10 W	–	–
waveguide	10 W	–	–
PULSED OUTPUT			
cw discharge, low pressure	1 kW	500	10-100
cw discharge, waveguide	5 kW	100	> 100
pulsed discharge, low pressure	5 kW	100	< 20
pulsed discharge, waveguide	10 kW	50	< 20
TEA	1 MW	100	< 1

APPENDIX E

INFRARED DETECTORS

INFRARED DETECTORS

Infrared detectors can be characterized as being one of two basic types. Thermal detectors, such as thermopiles and piezoelectrics, measure the heat produced by an incident infrared beam. Quantum detectors, namely photo-multipliers and photodetectors, respond to individual infrared photons. Thermal detectors have insufficient sensitivity and speed to be applied to high-resolution laser radars, and this appendix focuses on quantum detectors, specifically infrared photodetectors.

The feasibility of RMD has been greatly increased by recent developments in the area of IR photodetectors. Of particular significance are the improvements in focal plane array (FPA) technology[46],[47]. Detector arrays can reduce the requirements of scanners, laser pulse rates and the individual detection bandwidths of laser radar systems. FPAs allow for the combination of optical signal detection and electrical signal processing in the focal plane. Focal plane arrays are either monolithic or hybrid, and FPR signal processing requires that the photoelectric characteristics of the detector material be highly uniform and that the detector resistance be large.

Infrared imagers operate in one of the two separate wavelength bands which correspond to the minima in atmospheric attenuation, the mid-IR band between 3 and 5 μm, and the far-IR band between 8 and 13 μm. The 8 - 13 μm band is used to detect objects at near ambient temperatures, since at these temperatures the contrast is greater than that in the shorter wavelength band. However for hot bodies, such as the exhaust plumes of jet engines, the 3 - 5 μm band gives greater contrast and this spectral range is frequently used in heat-seeking missiles.

In the 1 to 6 μm wavelength range one may use Schottky barrier IR charge-coupled devices (CCDs) which are constructed of monolithic silicon and are available in large high-density arrays. These Schottky barrier arrays are relatively inexpensive since they are manufactured using standard IC processing techniques, and have a high degree of uniformity. Another possible detector material is extrinsic silicon, where the type and amount of the impurity determines the spectral characteristics of the detector. For operation below 6 μm the impurities are indium, sulfur and thalium and the detectors must be cooled to liquid nitrogen temperatures (77 K). At the longer 8 - 14 μm wavelengths silicon is doped with impurities such as magnesium, aluminum, and gallium to produce efficient detector arrays. Unfortunately these detectors operate at considerably lower temperatures than those in the 1 to 5 μm band, with typical cooling to below 30 K required. Cryogenic systems at these temperatures are impractical for an airborne RMD system.

Mercury Cadmium Telluride

The best detector material for use at the 10.6 μm wavelength of the RMD infrared laser radar is Mercury Cadmium Telluride (HgCdTe). The peak sensitivity of this alloy semiconductor can be adjusted between 1 μm and 50 μm by varying the ratio of mercury to cadmium. The Hg:Cd ratio determines the bandgap energy of the detector and the ability to vary this parameter is one of the reasons HgCdTe is such an attractive detector material. The spectral sensitivity is a maximum at 10.6 μm when the Hg:Cd ratio is 78:22.

In the 8 - 13 μm spectral band only hybrid FPAs are possible, with the HgCdTe detector substrate coupled to silicon CCDs. There are unfortunately no monolithic HgCdTe arrays at these longer wavelengths.

Injection efficiencies in hybrid HgCdTe devices approach 100%, with reverse resistances of the order of 20 MΩ. High reverse resistances reduce the electrical shot noise which occurs when the photodetectors are biased. One of the major problems to be overcome with FPA technology is the nonuniformity of the detector material and this must be corrected by signal processing.

Much of the work on advanced infrared FPA technology is motivated by the need to develop high-resolution IR sensors for military space-based systems, although FPA technology is also being applied to tactical military problems. The development of large HgCdTe FPAs has been directed exclusively at highly-classified military projects (mostly dealing with the Strategic Defence Initiative in the US) and it is difficult to assess the current state-of-the-art. The largest HgCdTe array reported to date is a 512 x 512 element FPA developed by Hughes Aerospace, and a 1024 x 1024 array was proposed for use in the TEAL RUBY program. Smaller arrays are much more common, such as 128 x 128 and 240 x 16. Longer arrays frequently have narrower aspect ratios, and the 1024 x 1 array used in the direct-detection RMD system is well within the reach of current technology, though not yet to the point of commercial availability.

Photodetector Theory

The current developed in a semiconductive photodetector is given by,

$$i = (\eta e / E_\lambda) P_s$$

where η is the quantum efficiency of the detector, e is the fundamental electron charge, P_s is the incident optical power, and E_λ is the photon

energy. The term ($\eta e/E_\lambda$) is known as the current responsivity of the photodetector and has the units of amps/Watt. The quantum efficiency is the ratio of the number of charge carriers formed to the incident photon flux. HgCdTe detectors typically have $\eta < 70\%$, with the specific quantum efficiency depending on the manufacturing process, elemental ratio and other factors. Photodetectors operate in one of two modes, either as photoconductors or as photodiodes. Mercury Cadmium Telluride (HgCdTe) infrared photodetectors are implemented as photoconductive PC HgCdTe or, more commonly, as photovoltaic PV HgCdTe. Hybrid infrared FPAs can only be implemented with PV HgCdTe. The characteristics of PC and PV detectors differ and both types are currently used for infrared laser radars systems. Typically HgCdTe photodetectors are cooled to liquid nitrogen temperatures (77 K) and have saturation values of the order of 1 mW.

PC detectors have greater sensivity than non-avalanching PV detectors because of the photoconductive gain, which is given by the ratio of the carrier lifetime to the carrier transit time. The longer carrier lifetime means that the response time of a photoconductor is of the order of 1 μsec. PV detectors are p-n junction devices with subnanosecond response times. Bandwidths of HgCdTe photodiodes can be in excess of 1 GHz. Unlike photoconductors there is no recombination noise in photodiodes since the charge carriers are swept away before they recombine, and hence the limiting noise of a PV detector can theoretically be a factor of $\sqrt{2}$ less than that of a PC detector.

There are many different sources of noise in infrared photodetectors:

- Johnson (a.k.a. thermal or Nyquist) noise
- 1/f (a.k.a. current, modulation, or excess) noise

- signal photon-induced shot noise
- background photon-induced shot noise
- thermal generation/recombination noise
- dark current shot noise.

Charge carriers in photodetectors are created optically by incident photons and thermally by phonon interactions. The statistical fluctuations in the rate of generation and recombination of these charge carriers is an important source of noise. Cooling the detector greatly reduces the problem of thermal generation/recombination and dark current shot noise. Photoconductors are frequently limited by the photon component of the generation/recombination noise. Infrared laser radars are usually operated at frequencies which are sufficiently high to make the 1/f noise negligible. However the Johnson noise, signal photon-induced shot noise, and background photon-induced shot noise often remain significant sources of noise for the infrared detectors used in CO_2 laser radars.

Johnson Noise

The random thermal motion of charge-carriers within the photo-detector generates electrical noise. The mean-square Johnson noise is

$$\langle i^2_{JN} \rangle = 4k_B T_e B/R$$

where k_B is the Boltzmann constant, T_e is the effective temperature in Kelvin, R is the zero-bias resistance and B is the bandwidth. The effective temperature is used to include the preamplifier noise factor F. If F is given in dB then the effective temperature is $T_e = T + 290[10^{F/10} - 1]$ where T is the actual temperature of the photodetector.

Signal Photon Shot Noise

The random nature of the arrival of signal photons at the detector results in shot noise. The mean-square value of this noise is

$$\langle i^2_{SN} \rangle = 2e^2 G^2 P_s B \eta / E_\lambda$$

where G is the detector gain. For ideal photodiodes G = 1, and the photovoltaic shot noise due to the signal photons is therefore

$$\langle i^2_{SN} \rangle = 2e^2 P_s B \eta / E_\lambda .$$

Background Photon Shot Noise

The shot noise is a photovoltaic detector due to the background photons is

$$\langle i^2_{BN} \rangle = 2e^2 P_B B \eta / E_\lambda$$

where P_B is the power of the background radiation. CO_2 laser radars, operating at 10.6 μm, can often be background-noise limited since this wavelength is at the peak of 300 K thermal emission. The background noise can be substantially reduced by using adequate spectral filtering.

Signal-to-Noise Ratio and Detectivity

If the signal photon-induced shot noise dominates the Johnson noise then the power signal-to-noise ratio (SNR) for a photovoltaic detector is

$$SNR = \eta P_s / BE_\lambda$$

and the noise-equivalent power (NEP) is

$$NEP = P_s / SNR = BE_\lambda / \eta.$$

This represents the quantum limit for an ideal back-biased photodiode. The detectivity of a photodetector is defined as being the reciprocal of the noise-equivalent-power, $D = 1/NEP$. In order to compare the performance of different infrared detectors one must normalize the detectivity for both the detector area and the electrical bandwidth. This D^* detectivity is given by $D^* = \sqrt{A_d B}/NEP$ where A_d is the area of the detector surface and B is the bandwidth of the detector system. D^* includes blackbody photon shot noise and Johnson noise and is a useful measure of the intrinsic properties of a given photodetector material. The detectivity of a photovoltaic detector will always be a factor of $\sqrt{2}$ greater than that of a comparable photoconductive detector because of the absence of recombination noise.

APPENDIX F

SCANNERS

SCANNERS

The design of an adequate scanning system is one of the most challanging aspects of any airborne infrared laser radar. The two basic types of scanning are object-space scanning (also known as full-aperture scanning) and image-space scanning. Object-space scanning is the situation where a laser beam spot and the instantaneous field-of-view of a detector are scanned over the target area. Image-plane scanning occurs when the image of the entire target area is swept across the detector. In general object-space scanners are able to cover a wider total field-of-view than their image space counterparts. Common object-space scanning devices are gimballed mirrors and rotating polygonal mirrors and wedges. Polygonal mirror scanners[4,8] are well-suited for the periodic, repetitive scanning required for a RMD system but they are by no means the only possible approach. Acousto-optic, galvanometric and holographic scanners can be used instead of, or in conjunction with, polygon mirrors to meet the demanding requirements of high-resolution airborne scanning.

Polygonal Scanners

Large, high-scan-rate polygonal mirrors are made of exotic materials such as beryllium rather than more common substances like aluminum. This is because mechanically strong and light materials are required in order to sustain the enormous centrifugal forces which tend to distort the mirror surfaces. High angular velocity scan mirrors also require sophisticated air bearings. The polygon wedges (prisms) used in image-plane scanning systems are frequently made from Germanium, and are subject to the same limitations as mirrors.

A polygonal mirror which is scanning a total scan angle of θ is shown in Figure F.1. For continuous scanning the scan angle must equal the facet angle. The size of the facet is determined by the diameter of the beam. A facet angle of 7.5°, which corresponds to a 48-faceted polygon, gives a total scan coverage of 15°. A facet length of 8 mm corresponds to a polygon radius of 6 cm. Acousto-optic scanners are often combined with rotating polygons to deflect an incident laser beam onto the center of each facet during the entire duration of a scan. This reduces the size of the facet needed and hence the overall size and cost of the polygon.

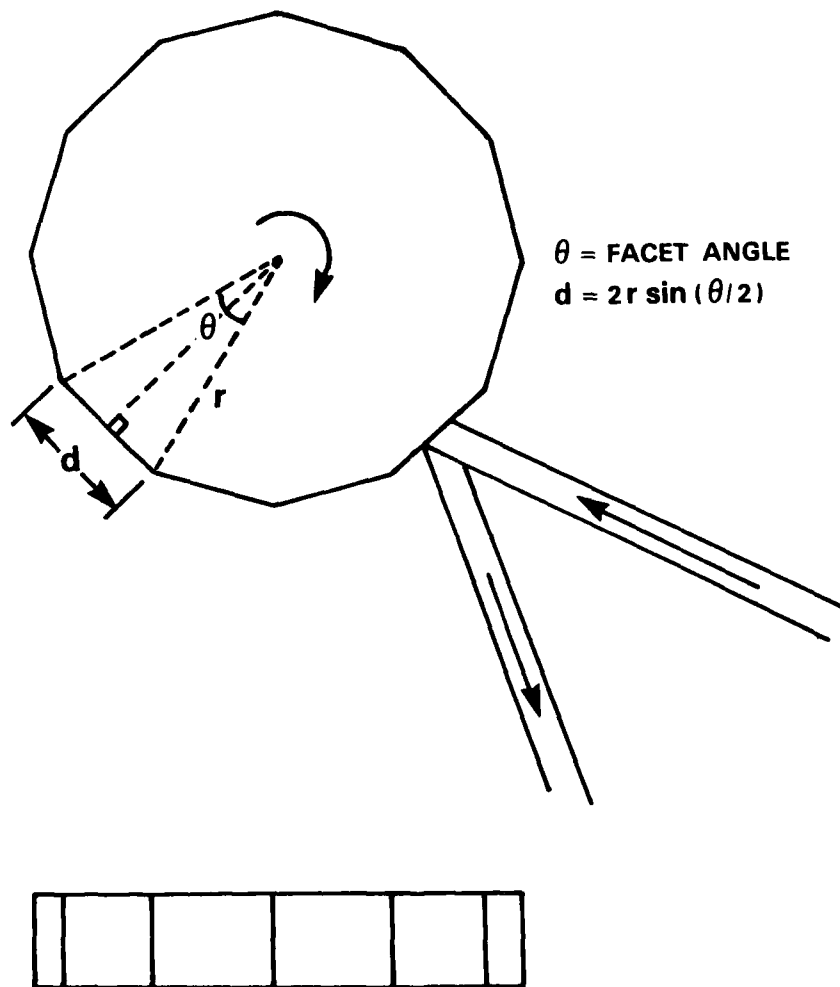θ = FACET ANGLE

$d = 2r\sin(\theta/2)$

Figure F.1

POLYGONAL SCANNING MIRROR

APPENDIX G

STANDARD INFRARED DIFFUSE TARGETS

STANDARD INFRARED DIFFUSE TARGETS

The need for diffuse reference targets in the calibration of CO_2 lidars has resulted in the development of a number of standard target materials. These standard targets have been studied and used extensively by a number of groups working with CO_2 laser radars. The reflection and polarization characteristics of calibration targets are established as part of the overall lidar system calibration. Many surfaces which are diffuse at visible wavelengths are specular in the thermal infrared so that new diffuse targets have had to be developed for use at 10.6 µm.

The standard targets presented in the appendix are all, to a greater or lesser extent, diffuse (Lambertian) surfaces. The ideal reference diffuse target would be one with a high reflectance, i.e., ρ nearly equal to one, and a Lambertian intensity distribution. In-depth diffusers, such as slurried salt, have almost perfect Lambertian characteristics while surface diffusers, like sand-blasted aluminum, tend to demonstrate specular peaks in an otherwise diffuse distribution. Standard diffuse targets for CO_2 laser radars are all depolarizing to some degree but are not perfectly diffuse. If an incident laser beam is linearly polarized in a particular direction this component remains dominant in the reflected radiation. Two of the most common in-depth diffusers are sulfur and slurried salt, while flame-sprayed aluminum, sand-blasted aluminum and silicon carbide sandpaper are among the best surface diffusers. The preparation and characteristics of three types of diffuse targets are presented below. It must be emphasized that the reflectivity of all diffuse targets used at CO_2 laser wavelengths depends to a great extent on the method of preparation, and this can vary substantially. Weathering, dirt and moisture are also important

considerations. Much work is currently directed at developing better, more "standard" diffuse targets, especially for use with mobile laser radar systems operating in a multitude of environments.

References in the literature which give 10.6 μm reflectance data for standard targets and for a variety of other materials are listed in Table G.1.

Sulfur

This is prepared by mixing sublimed sulfur powder with alcohol. Sublimed sulfur is commonly referred to as "flowers of sulfur". The mixture is pressed into a shallow holder and the alcohol evaporated to leave a smooth, flat sulfur surface. Sulfur is a good reference target for wavelengths in the 9 - 11 μm range because its reflectivity shows very little wavelength dependence. Sulfur has a hemispherical total reflectance of $\rho = 0.8$ at 10.6 μm. Unfortunately sulfur targets cannot be used for CW laser powers exceeding 1 W/cm² because the absorption at these power levels is sufficient to melt the sulfur.

Slurried Salt

Salt (NaCl) is transparent at 10 μm and a cake of salt crystals acts as an in-depth diffuser with the resultant reflectance being almost perfectly Lambertian. Pure NaCl granules are slurried with an equal volume of water in a high-chromium stainless-steel container and baked dry for two weeks at 80°C. A salt target must be kept above 55°C during use to prevent water absorption. At 10.6 μm a slurried salt target has a reflectance of between 75% to 85%.

TABLE G.1

REFERENCES TO 10.6 μm REFLECTANCE DATA

Standard CO_2 Laser Radar Targets

Aluminum	3-5, 8, 10, 11, 15, 23, 49, 52, 55, 57, 58
Sodium Chloride	32, 50, 57
Sandpaper	3, 5, 13, 49, 51, 52, 54
Gold	1, 5, 32, 49, 50, 52, 57
Sulfur	3, 5, 12, 13, 49-51, 53, 54, 57

Other Materials

Asphalt	5, 10, 11, 23, 55
Concrete	5, 8, 55, 58
Fiberglass	5, 58
Graphite	50, 58
Ice	4, 5, 58
Paint	4, 5, 10-12, 23, 41, 58
Paper	58
Quartz	27, 32
Rock	1, 10, 11, 25-27, 32, 55-57
Snow	1, 5, 10, 56, 58
Soil	1, 8, 11, 23, 25-27, 56, 58
Vegetation	1, 5, 8, 11, 23, 26, 56, 58
Water	1, 5, 10, 58

Flame-Sprayed Aluminum

This is one of the most commonly-used standard diffuse targets
in the thermal infrared. It is prepared by first sandblasting an
aluminum plate and then priming the surface with a flame-sprayed layer
of nickel. A coating of pure alumina (aluminum oxide) is then
deposited by flame-spraying. The reflectance of this surface is Lam-
bertian, with a albedo of the order of 60% and 15% depolarization.
Flame-sprayed aluminum has been found to weather well and serves as the
calibration target for many military infrared radar systems.

APPENDIX H

DOPPLER EFFECT

DOPPLER EFFECT

The Doppler effect is the shift in the frequency of radiation due to the motion of a target with respect to a detector. For many military laser radar systems the Doppler effect provides an excellent means of moving-target indication (MTI) and velocity determination. In terms of remote minefield detection, where the targets are stationary, the Doppler effects are merely inconvenient. A radial velocity $\vec{v}_R$ introduces a frequency shift

$$\Delta\nu = (2/\lambda)v_R$$

where λ is the emitted laser wavelength. At the CO_2 laser wavelength of 10.6 μm the Doppler shift is $\Delta\nu = 189$ kHz/ms^{-1}. For the situation of a moving aircraft the frequency shift is due to the component of relative velocity parallel to the radiation which, as shown in Figure H.1, is $v_R = v_A\sin\theta$.

If the airborne lidar is imaging a target which is moving with a velocity $\vec{v}_T$ the frequency shift becomes

$$\Delta\nu = (2/\lambda)[|\vec{v}_T + \vec{v}_A|]\sin\theta.$$

The Doppler effect is also important in any lidar system which makes use of a scanning mirror. The motion of the mirror introduces frequency shifts which broaden the system bandwidth and limit the ultimate Doppler resolution of the laser radar. Consider the scanning arrangement of Figure H.2, where the mirror is oscillating about its center with an angular velocity of ω and an amplitude of θ_m. The Doppler shift at a given point P on the surface of the mirror is
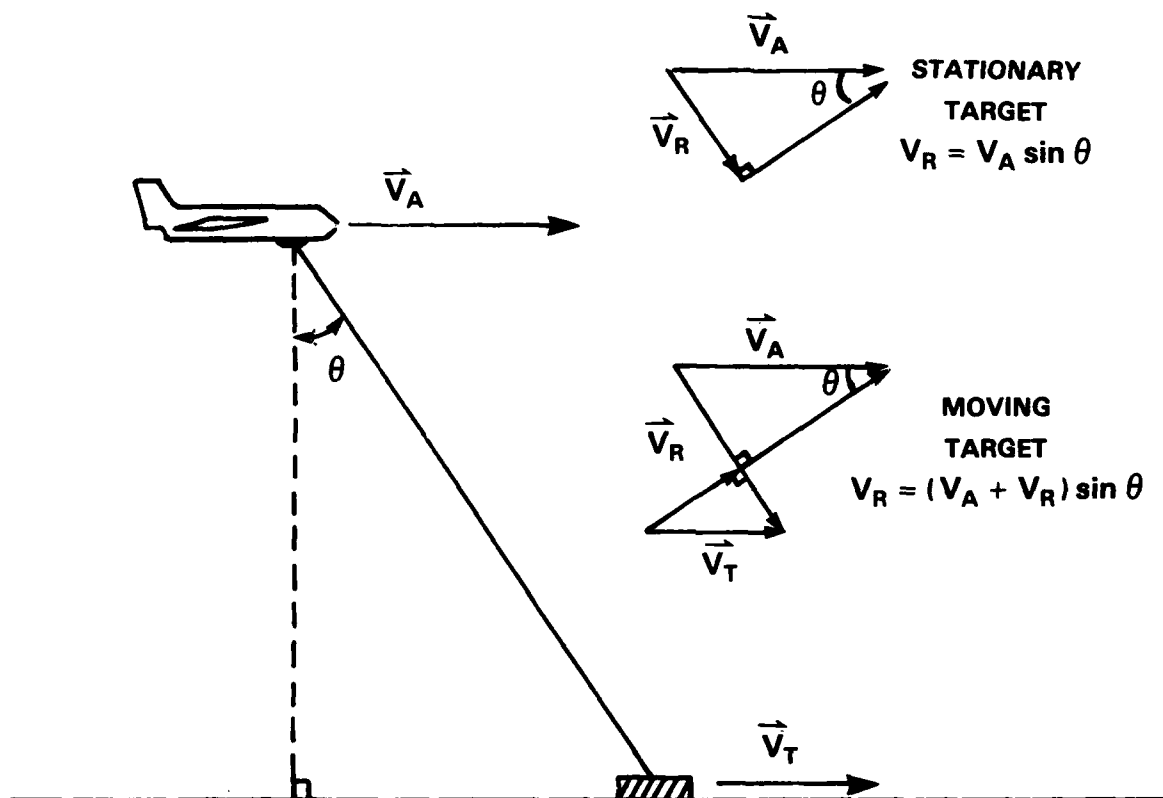
Figure H.1

AIRBORNE LASER RADAR IMAGING A GROUND TARGET

$$\theta = \theta_m \sin \omega t$$

$$V_P = r \frac{d\theta}{dt} = r\theta_m \omega \cos \omega t$$

$$V_R = V_P \cos \theta$$
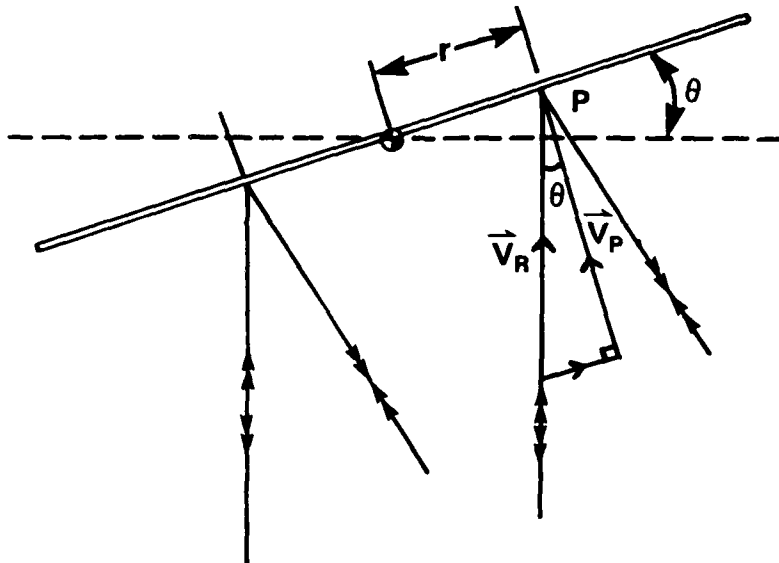
Figure H.2

MOTION OF A SCANNING MIRROR SURFACE

$$\Delta\upsilon = (2/\lambda)r\theta_m\omega\cos\theta\cos(\omega t)$$

where r is the radial distance of the point P from the centre of the rotation. For a beam diameter of D the rms value of the Doppler broadening is

$$\Delta\upsilon = (2\sqrt{2}/\lambda)D\theta_m\omega.$$

The expression above assumes that there are two bounces off the mirror, one upon transmission and the other during reception.

APPENDIX I

RANDOM NUMBER GENERATION

RANDOM NUMBER GENERATION

It is often necessary to generate a set of random numbers which are distributed according to some specific distribution. The effect of speckle on a RMD system can be modelled by using the known statistical properties of speckle patterns. There are several ways of obtaining random numbers which follow a specific probability distribution, and two of the most useful the inverse method and the direct method.

Inverse Method

Given a set of numbers which follow a uniform distribution one can generate numbers which obey any other probability distribution through the use of the cumulative distribution function. Let $f(y)$ be the probability density function of some arbitrary distribution. Then the cumulative distribution function is given by

$$F(y) = \int_{-\infty}^{y} f(y)dy.$$

If the random variable, U, is uniformly distributed on the unit interval [0,1], and if $F_X(x)$ is the cumulative distribution function for the random variable, X, then setting each

$$u = F_X(x)$$

will give a value x. The inverse method requires that the function $F_X(x)$ be readily invertible. For example a negative exponential distribution is described by the probability density function

$$f(x) = 1/\theta \exp[-x/\theta]$$

where θ is a constant. The cumulative distribution function is therefore

$$F_X(x) = 1 - \exp[-x/\theta].$$

Equating this to each value, u, gives an element of the negative exponential

$$x = -\theta \ln[1 - u].$$

The uniformly-distributed values U[0,1] can be obtained from a straight-forward random number generator, which is a standard function available on most computers. FORTRAN-77 provides the RAN function which uses the multiple congruential method to generate a pseudo-random U[0,1] distribution.

Direct Method

Many distributions do not have an easily invertible cumulative distribution function. For instance the normal probability distribution function is

$$f_X(x) = 1/\sqrt{2\pi}\sigma \exp[-(x - \bar{x})/2\sigma^2]$$

where $\bar{x}$ is the mean and σ^2 is the variance. The corresponding cumulative distribution is

$$F_X(x) = 1/\sqrt{2\pi}\sigma \int_{-\infty}^{x} \exp[-(x - \bar{x})/2\sigma^2] dx.$$

Normally distributed (Gaussian) random numbers can be generated using the direct method[59]. If u_1 and u_2 are a pair of uniformly-distributed random numbers from $U[0,1]$ the number

$$n = \sqrt{-2\ell n u_1}\cos(2\pi u_2)$$

is a value from the zero mean, unit variance normal distribution $N(0,1)$. This can be adjusted to the required normal distribution, $N(\bar{x},\sigma^2)$ through the relation

$$x = \sigma n + \bar{x}.$$

Another simpler algorithm uses the fact that if $u_{i=1,12}$ are twelve random numbers from $U[0,1]$ then the number

$$n = \sum_{i=1}^{12} u_i$$

is Gaussian with a mean of 6 and a variance of 1. Again this can be normalized to give the required $N(\bar{x},\sigma^2)$ distribution.

APPENDIX J

LIST OF ACRONYMS

LIST OF ACRONYMS

BLIP	=	Background-Limited Photodetector
BRDF	=	Bidirectional Reflectance Distribution Function
CCD	=	Charge-Coupled Device
CW	=	Continuous Wave
DIAL	=	Differential Absorption Lidar
FLIR	=	Forward-Looking Infrared
GCS	=	Ground Control Station
IF	=	Intermediate Frequency
IFOV	=	Instantaneous Field-of-View
INS	=	Inertial Navigation System
IRAR	=	Infrared Airborne Radar
IRLS	=	Infrared Line Scan
IR/EO	=	Infrared Electro-Optics
IR STARTLE	=	Infrared Surveillance and Target Acquisition Radar
LADAR	=	Laser Detection and Ranging (Laser Radar)
LATAS	=	Laser True Air Speed
LIDAR	=	Light Detection and Ranging
LIRS	=	Laser Imaging Radar Sensor
LO	=	Local Oscillator
LOTAWS	=	Laser Obstacle/Terrain Avoidance Warning System
LRF	=	Laser Rangefinder
MICOS	=	Multifunction Infrared Coherent Optical Sensor
MTI	=	Moving Target Indication
NEP	=	Noise Equivalent Power
PC	=	Photoconductive
PRF	=	Pulse Repetition Frequency
PV	=	Photovoltaic
RMD	=	Remote Minefield Detection

SNR   = Signal-to-Noise Ratio

SPRITE   = Signal Processing in the Element

TDI   = Time-Delay Integration

TEA   = Transversely Excited Atmospheric

Establishments, institutions, companies and societies:

AFGL   - Air Force Geophysics Laboratory (US)

CCRS   - Canadian Center for Remote Sensing (Canada)

DRES   - Defence Research Establishment Suffield (Canada)

DREV   - Defence Research Establishment Valcartier (Canada)

IEE   - Institute of Electrical Engineers (UK)

IEEE   - Institute of Electrical and Electronics Engineers (US)

ERIM   - Environmental Research Institute of Michigan (US)

FA   - Ford Aerospace (US)

MIT   - Massachusetts Institute of Technology (US)

MM   - Martin Marietta (US)

NAR   - North American Rockwell (US)

NOAA   - National Oceanic and Atmospheric Administration (US)

NDRI   - National Defence Research Institute (Sweden)

PDS   - Pilkington Defence Systems (Barr and Stroud, UK)

RSRE   - Royal Signals and Radar Establishment (UK)

SPIE   - International Society for Optical Engineering (US)

UTRC   - United Technologies Research Center (US)

APPENDIX K

CONSTANTS AND CONVERSION FACTORS

CONSTANTS AND CONVERSION FACTORS

Constants

Boltzmann's constant, k_B = 1.38(10^{-23}) J/K

Planck's constant, h = 6.626(10^{-34}) Js

Electron charge, e = 1.602(10^{-19}) C

Speed of light, c = 2.998(10^{9}) m/s

Stefan's constant, σ = 5.67(10^{8}) Wm^{-2}K^{-4}

Conversion Factors

1° = 17.45 mrad   1 km/hr = 0.278 m/s

1 eV = 1.602(10^{-19}) J   10 μm ⟷ 30 THz

DOCUMENT CONTROL DATA - R & D

(Security classification of title, body of abstract and indexing annotation must be entered when the overall document is classified)

1 ORIGINATING ACTIVITY	2a. DOCUMENT SECURITY CLASSIFICATION
Defence Research Establishment Suffield	Unclassified
	2b. GROUP

3 DOCUMENT TITLE

Remote Minefield Detection Using Infrared Laser Radar (U)

4 DESCRIPTIVE NOTES (Type of report and inclusive dates) Suffield Memorandum

5. AUTHOR(S) (Last name, first name, middle initial)

Stuart, Gregory C.

6. DOCUMENT DATE November 1988	7a. TOTAL NO. OF PAGES 128	7b. NO. OF REFS 59
8a. PROJECT OR GRANT NO. 031SD	**9a. ORIGINATOR'S DOCUMENT NUMBER(S)** SM 1223	
8b. CONTRACT NO.	**9b. OTHER DOCUMENT NO.(S) (Any other numbers that may be assigned this document)**	

10. DISTRIBUTION STATEMENT

Unlimited

11. SUPPLEMENTARY NOTES	12. SPONSORING ACTIVITY

13. ABSTRACT

High-resolution infrared laser radars are shown to be effective sensors for use in remote minefeld detection (RMD). The theoretical aspects and practical limitations of imaging laser radars are discussed and the conceptual designs of two airborne carbon-dioxide laser radars are presented. A design which uses direct detection and a linear-array detector is shown to be superior to one using heterodyne detection and a single-element detector. Countermeasures to active infrared RMD systems are discussed and suggestions made for further study.

KEY WORDS

laser radar
infrared
remote sensing
minefield detection
active IR
CO_2 lasers

INSTRUCTIONS

1. ORIGINATING ACTIVITY Enter the name and address of the organization issuing the document.

2a. DOCUMENT SECURITY CLASSIFICATION: Enter the overall security classification of the document including special warning terms whenever applicable.

2b. GROUP Enter security reclassification group number. The three groups are defined in Appendix 'M' of the DRB Security Regulations.

3. DOCUMENT TITLE Enter the complete document title in all capital letters. Titles in all cases should be unclassified. If a sufficiently descriptive title cannot be selected without classification, show title classification with the usual one-capital-letter abbreviation in parentheses immediately following the title.

4. DESCRIPTIVE NOTES Enter the category of document, e.g. technical report, technical note or technical letter. If appropriate, enter the type of document, e.g. interim, progress, summary, annual or final. Give the inclusive dates when a specific reporting period is covered.

5. AUTHOR(S): Enter the name(s) of author(s) as shown on or in the document. Enter last name, first name, middle initial. If military, show rank. The name of the principal author is an absolute minimum requirement.

6. DOCUMENT DATE. Enter the date (month, year) of Establishment approval for publication of the document.

7a. TOTAL NUMBER OF PAGES: The total page count should follow normal pagination procedures, i.e., enter the number of pages containing information.

7b. NUMBER OF REFERENCES Enter the total number of references cited in the document.

8a. PROJECT OR GRANT NUMBER If appropriate, enter the applicable research and development project or grant number under which the document was written.

8b. CONTRACT NUMBER If appropriate, enter the applicable number under which the document was written.

9a. ORIGINATOR'S DOCUMENT NUMBER(S) Enter the official document number by which the document will be identified and controlled by the originating activity. This number must be unique to this document.

9b. OTHER DOCUMENT NUMBER(S): If the document has been assigned any other document numbers (either by the originator or by the sponsor), also enter this number(s).

10. DISTRIBUTION STATEMENT: Enter any limitations on further dissemination of the document, other than those imposed by security classification, using standard statements such as:

   (1) "Qualified requesters may obtain copies of this document from their defence documentation center."

   (2) "Announcement and dissemination of this document is not authorized without prior approval from originating activity."

11. SUPPLEMENTARY NOTES: Use for additional explanatory notes.

12. SPONSORING ACTIVITY: Enter the name of the departmental project office or laboratory sponsoring the research and development. Include address.

13. ABSTRACT: Enter an abstract giving a brief and factual summary of the document, even though it may also appear elsewhere in the body of the document itself. It is highly desirable that the abstract of classified documents be unclassified. Each paragraph of the abstract shall end with an indication of the security classification of the information in the paragraph (unless the document itself is unclassified) represented as (TS), (S), (C), (R), or (U).

The length of the abstract should be limited to 20 single-spaced standard typewritten lines; 7½ inches long.

14. KEY WORDS. Key words are technically meaningful terms or short phrases that characterize a document and could be helpful in cataloging the document. Key words should be selected so that no security classification is required. Identifiers, such as equipment model designation, trade name, military project code name, geographic location, may be used as key words but will be followed by an indication of technical context.